

**TRIBOELECTRIC NANOGENERATORS:
BIOMECHANICAL ENERGY HARVESTING,
SELF POWERED SENSOR AND WEARABLE
APPLICATIONS**

A THESIS SUBMITTED TO
THE GRADUATE SCHOOL OF ENGINEERING AND SCIENCE
OF BILKENT UNIVERSITY
IN PARTIAL FULFILLMENT OF THE REQUIREMENTS FOR
THE DEGREE OF
MASTER OF SCIENCE
IN
MATERIALS SCIENCE AND NANOTECHNOLOGY

By
Ahmet Faruk Yavuz
September, 2017

TRIBOELECTRIC NANOGENERATORS: BIOMECHANICAL
ENERGY HARVESTING, SELF POWERED SENSOR AND
WEARABLE APPLICATIONS

By Ahmet Faruk Yavuz

September, 2017

We certify that we have read this thesis and that in our opinion it is fully adequate,
in scope and in quality, as a dissertation for the degree of Master of Science.

Hasan Tarık Baytekin (Advisor)

Mehmet Bayındır (Co-Advisor)

Şemsettin Türköz

Talip Serkan Kasırga

Approved for the Graduate School of Engineering and Science:

Ezhan Karaşan

Director of the Graduate School

ABSTRACT

TRIBOELECTRIC NANOGENERATORS: BIOMECHANICAL ENERGY HARVESTING, SELF POWERED SENSOR AND WEARABLE APPLICATIONS

Ahmet Faruk Yavuz

M.S. in Materials Science and Nanotechnology

Supervisor: Hasan Tarık Baytekin

September, 2017

One of the biggest challenges ahead massive advancement of electronic technology is increasing energy consumption. A closer consideration on draining of fossil reserves and rapid development of wearable and portable consumer electronics, inevitable paradigm shift is required towards use of renewable energy sources and self-powered electronic systems respectively. In parallel to this consideration, triboelectric nanogenerators have emerged to scavenge energy from ambient environment by using ubiquitous phenomenon of triboelectricity or contact electrification in other words. Essentially, triboelectric nanogenerators harvest mechanical energy into electricity by utilizing triboelectric charge generation and electrostatic induction phenomenon. Accordingly, we developed high performance biomechanical energy harvesting floor tiles to scavenge human motions into electricity and electrode core-polymer shell structured triboelectric nanogenerator fibers for wearable applications. Furthermore, new perspectives are introduced for fabrications of low-cost, mass producible, large area and flexible triboelectric nanogenerator structures.

Keywords: Triboelectricity, energy harvesting, self-powered sensors, wearable electronics, thermally fiber drawing.

ÖZET

TRIBOELEKTRİK NANOJENERATÖRLER: BİYOMEKANİK ENERJİ HASATLAMA, KENDİ GÜCÜNÜ SAĞLAYAN SENSÖRLER VE GIYİLEBİLİR UYGULAMALAR

Ahmet Faruk Yavuz

Malzeme Bilimi ve Nanoteknoloji Yüksek Lisans Tezi

Tez Danışmanı: Hasan Tarık Baytekin

Eylül, 2017

Elektronik teknolojisindeki kayda değer ilerlemenin önündeki en büyük zorluklardan biri de artan enerji tüketimidir. Fosil yakıtların hızla tükenmesi ve taşınabilir ile giyinebilir tüketici elektroniğinin hızla gelişmesi göz önünde bulundurulursa, sırasıyla yenilebilir enerji kaynaklarına ve kendi enerjisini sağlayan elektronik sistemlere doğru kaçınılmaz bir paradigma değişimine ihtiyaç gerekmektedir. Triboelektrik nanojeneratörler, bu düşünceye paralel olarak yaşadığımız çevreden enerji üretmek amacıyla, her yerde nazır olan triboelektriği ya da bir diğer tabirle sürtünme ile elektriklenmeyi kullanarak ortaya çıktılar. Temelde, triboelektrik nanojeneratörler, sürtünme elektriklenmeyi ve elektrostatik endüksiyonu kullanarak mekanik enerjiyi elektriğe çevirmektedirler. Bu mekanizmadan yola çıkarak, biz de insan hareketlerini elektriğe dönüştürmek için yüksek performanslı biyomekanik enerji hasatlayıcı zemin döşemelerini ve giyilebilir uygulamalar için merkezde elektrot-kabukta polimer yapısında olan triboelektrik nanojeneratör ip-liklerini geliştirdik. Ayrıca, düşük maliyetli, seri üretilebilir, geniş alanlı ve esnek triboelektrik nanojeneratör yapılarının üretimi için yeni bakış açıları sunduk.

Anahtar Kelimeler: Triboelektrik, enerji hasatlama, kendi gücünü sağlayan sensörler, giyilebilir elektronik, ısısal fiber çekme.

Acknowledgement

I would like to thank my academic advisor, Asst. Prof. Hasan Tarık Baytekin and co-advisor, Prof. Mehmet Bayındır for their support and guidance throughout my studies. They provided me a rich research environment, so I had chance to improve my research skills in depth.

In particular, I give my special thanks to, Arbab M. Toufiq, Abba Usman Saleh, Umar Gishiwa Musa, Abubakar Isa Adamu, Pınar Beyazkılıç, Muhammad Yunusa and M. Girayhan Say who helped steer the wheel with me all the time and reach out to me whenever I need their assistance.

I would like to thank the entire faculty and management members at UNAM-National Nanotechnology Research Center who provided me world-class research infrastructure and facilities in this journey. In particular, I am so grateful to Murat Dere for his fervent support throughout this journey.

I would like to express sincere gratitude to my beloved family, especially my wife and daughter who have made sacrifice for our success. I am so grateful to them, including my mother, father and sisters for their prayers and support in my life.

Contents

Chapter 1	Introduction	1
Chapter 2	Background.....	3
2.1.	Triboelectricity	3
2.2.	Triboelectric Series	4
2.3.	Theory of Triboelectricity	7
2.3.1.	Electron Transfer.....	8
2.3.2.	Ion Transfer.....	9
2.3.3.	Material Transfer.....	10
2.4.	Applications of Triboelectricity and Triboelectric Nanogenerators	11
2.5.	Operation Modes of Triboelectric Nanogenerators	13
2.5.1.	Contact-Separation Mode	14
2.5.2.	Sliding Mode.....	16
2.5.3.	Single Electrode Mode.....	17
2.5.4.	Free-Standing Triboelectric Layer Mode.....	18
2.6.	Fabrication and Characterization of Triboelectric Nanogenerators....	19
2.7.	Applications of Triboelectric Nanogenerators.....	22
2.7.1.	Large Scale Energy Harvesting.....	22
2.7.2.	Mobile and Portable Energy Harvesting.....	23

2.7.3. Self-Powered Sensors	25
2.7.4. Tribotronics	26
Chapter 3 High Performance and Large Area Biomechanical Energy Harvesting Floor Tiles.....	27
3.1. Introduction	27
3.2. Effects of Device Structure and Material Properties on Output Performance of Triboelectric Nanogenerators	28
3.2.1. Working Mechanism of Contact Separation Mode.....	28
3.2.2. Optimization of Surface Modification Technique	31
3.3. Fabrication of Large Area Triboelectric Nanogenerator Floor Tiles ..	35
3.3.1. Material Selections and Surface Treatment Optimizations.....	35
3.3.2. Device Structure.....	42
3.4. Characterization	44
Chapter 4 Triboelectric Nanogenerator Fabrics	47
4.1. Introduction	47
4.2. Fabrication of Triboelectric Nanogenerator Fibers.....	49
4.2.1. Fiber Drawing	49
4.2.2. Surface Modification and Device Fabrication	53
4.3. Characterization	54
Chapter 5 Conclusions	55
5.1. Conclusion	55
5.2. Future Works.....	56
Bibliography.....	58

List of Figures

Figure 2.1: Triboelectrification in environment: (a) Volcanic lightning during Chaitin volcano eruption, 2008 [13]. (b) Dust devil on Mars is observed by Spirit rover, 2005 [14]. 4

Figure 2.2: Schematics of the proposed triboelectrification mechanisms. (a) Electron transfer mechanism, in which electrons are exchanged due to different work functions of materials. (b) Ion transfer mechanism, strongly bounded fixed ions and mobile counter ions are represented as positive and negative polarities respectively, in which mobile ions are transferred after intimate contacts. (c) Material transfer mechanism, in which charge generation is originated from transferred material species. 7

Figure 2.3: Electron transfer between metal-metal contact..... 8

Figure 2.4: “Mosaics” of generated triboelectric charge potentials are scanned via KFM [29]. Polydimethylsiloxane (PDMS) surface potential maps (a) before contact, (b) after intimate contact with Polycarbonate (PC). 11

Figure 2.5: Schematics of TENG operation modes. (a) Contact-separation mode. (b) Sliding mode. (c) Single electrode mode. (d) Free standing triboelectric layer mode. 13

Figure 2.6: Working mechanism of contact-separation mode. (a) Pressing step in which external force brings the two insulators into contact, resulting in triboelectric charge generation on surfaces. (b) Releasing step leads induced electron flow between electrodes. (c) Re-pressing by external force leads electron backflow due to potential difference variation. (d) Intimate contact step is established again in which electron flow reaches equilibrium. 15

Figure 2.7: Working mechanism of sliding mode. (a) Lateral sliding via external force initiates induced electron flow. (b) Full separation of insulators results in electron flow saturation. (c) Backward sliding yields electron backflow to balance

electrostatic potential drop. (d) Complete contact step in which electrostatic potential difference vanishes zero.	16
Figure 2.8: Working mechanism of single electrode mode. (a) Contact and separation of human skin generate electrostatic potential difference which yields electron flow through external load (b) When critical separation is supplied system comes into equilibrium. (c) While human skin coming closer to PTFE layer, electrostatic potential drop is emerged which results in backflow of electrons. (d) Complete contact condition is established again in which electron flow reaches equilibrium.	17
Figure 2.9: Effect of surface morphology on TENG output performance [98]. Scanning electron microscope images of (a) plain polyethylene terephthalate (PET) film, (b) plain PDMS film, (c-g) surface structured PDMS films.	21
Figure 2.10: Application areas of TENGs [166] . (a) TENG as a biomechanical energy harvester and power source for small scale electronics. (b)Energy harvesting from environment by TENGs and their promising application areas.	24
Figure 3.1: Vertical contact separation mode TENG device structures. (a) Dielectric-dielectric layered. (b) Metal-dielectric layered.	29
Figure 3.2: SEM micrographs of (a) PC nanopillars fabricated by AAO mold (b) PC nanopillars fabricated by Si mold (c-d) step 2 micro/nano CPE wires.	32
Figure 3.3: Step 2 CPE micro-nano wire preparation. (a) Step 2 CPE-PC/PSU core-shell fibers. (b) Chemical etching of fibers. (c) Electrostatic interaction of etched CPE micro-nanowires with PTFE rod. (d) Step 2 CPE micro-nano wire triboelectric layer.	33
Figure 3.4: Output characteristics of different surface structured TENGs and current-voltage measurement system.	34
Figure 3.5: Argon plasma surface modification system and mechanism (a) Microwave sourced vacuum chamber (b) Schematic of Ar ions collision with polymer surface.	35

Figure 3.6: Triboelectric series constructed through relative electrostatic potential measurement by electrostatic fieldmeter.	36
Figure 3.7: Ar plasma surface treatment optimization of (a) PC, PEI, PES, PEST, PSU, (b) CPE and PTFE films. (c) Contact angle images of polymer surfaces before and after plasma surface modifications, 5 min and 240 W for PC, PEI, PES, PEST, PSU films and 240 min, 600 W for CPE and PTFE films.	37
Figure 3.8: AFM images of polymer surfaces before and after plasma surface treatment process.	39
Figure 3.9: Fabrication and characterizations of miniature TENGs. (a) Preperation of triboelectric layers of TENG. (b) Custom made tapping device. (c) 3D printed TENG construction.	40
Figure 3.10: Output performance comparisons of flat polymer films (output-F) and Ar plasma surface treated polymer films (output-PT) based TENGs. (a) Short circuit current measurement results. (b) Open circuit voltage measurements.	41
Figure 3.11: Large area TENG floor tiles. (a) 3D sketch of device structure. (b) Fabricated proof of principle device.	43
Figure 3.12: Working mechanism of energy harvesting floor tiles. (1) Initial contact step triggered by external mechanical source in which triboelectric charge generation takes place, (2) Self-separation of triboelectric layers when external force leaves results in electrostatic induction between conductive polymer and electrode, (3) Induced charges come into equilibrium at full separation, (4) Re-pressing over floor tiles leads electrostatic potential differentiation, and hence backflow of induced charges are initiated, (5) When separation gap distance vanish to zero which also being at means full contact state, induced charge flow come into equilibrium.	44
Figure 3.13: Output characterization of device. (a) Schematics of voltage and current measurement setups. (b) 3D sketch of TENG floor tiles. (c) Hand press over device instantaneously powered 600 green and blue LED. (d) Open circuit output voltages generated by TENG under single footsteps with different weighted biomechanical loads.	45

Figure 3.14: Output performance of TENG floor tiles. (a) Short circuit current and (b) open circuit voltage measurement at 7 Hz tapping frequency. (d) Frequency dependent output currents (2-8 Hz).....	46
Figure 4.1: Thermal fiber drawing process. (a) Polymer film rolling over high melting point rod. (b) Custom made fiber drawing tower. (c) Preform is placed into furnace by preform holder.....	49
Figure 4.2: CPE-PC fiber drawing. (a) CPE and PC films. (b) PC preform after consolidation process. (c) CPE-PC fiber. (d) Roll of CPE film is placed into PC preform.	50
Figure 4.3: Iterative size reduction fiber drawing process. (a) Schematics of step-1 and step 2 fiber drawing. (b) SEM micrograph of step-1 CPE-PC core-shell fiber cross section. (c) Step-2 CPE-PC/PSU and (d) step-1 CPE-PC preforms after fiber drawing processes.	51
Figure 4.4: Metal core-polymer encapsulated fibers. (a) Preparation of solder rod. (b) End of fiber drawing process, melted solder rod within PSU preform. (c) SEM micrograph of $Pb_{67}Sn_{33}$ -PES core-shell fiber cross section.	52
Figure 4.5: Surface modification for thermally drawn fibers and device structure. (a) Schematic of Ar plasma surface treatment on CPE-PC core-shell fiber. (b) Rolled fibers over plasma sample holder cylinders. (c) The proof of principle textile TENG.	53
Figure 4.6: Output characteristics of textile TENG. Measurement results of (a) short circuits current, (b) open circuit voltage.....	54

List of Tables

Table 1: Comparison of triboelectric series in different studies [22]..... 6

Chapter 1

Introduction

The drastic development of technology over past centuries bring along rapidly increasing high-energy consumption. According to reports of World Energy Council [1], ninety percent of world energy consumption based on non-renewable sources which are limited to be supplied in the future, and cause irreversible damage on nature of earth. In this case, utilizing of renewable sources such as wind, solar and hydropower have emerged as an alternative supply for world energy demand in clean, sustainable and green ways. On the other hand, miniaturization on personal electronics has been bringing about mobile, portable, self-chargeable and wearable power sources demands. In parallel to these considerations, triboelectric nanogenerators (TENGs) have emerged as a sustainable, renewable and flexible energy harvesting devices. Essentially TENGs harvest mechanic energy into electricity through utilizing triboelectrification of materials and electrostatic induction phenomena. Promising scavenging energy capabilities of TENGs lead to be used in many of application area including large-scale energy harvesting, mobile and portable power source and self-powered sensors as well.

Fabrication of energy harvesting structures and developing efficient applications are major considerations of TENG research. As being a promising candidate

of large scale, renewable and sustainable energy harvester, developing mass producible, cost-effective and large area TENG structures have been gaining attention. On the other hand, novel fabrication methods should also be capable to produce flexible, transparent and textile structures as well especially for mobile and portable application of TENG.

Chapter 2

Background

2.1. Triboelectricity

Triboelectricity is a conceptually well-known phenomenon throughout history. Reports date back to 2400 years ago, a discovery experiment of Thales of Miletus on contact electrification who observed that amber and cat's fur are electrified when rubbed each other [2-4]. Thus, etymology of 'triboelectric' originated from Greek words of τριβ (tribo) and ἤλεκτρον (elektron) meaning rub and amber respectively addresses to rubbing amber [5,6].

Essentially, whenever two materials are brought into contact and separated afterwards, surface of materials are charged oppositely which is called as triboelectric effect, triboelectrification or contact electrification. It is mostly seen in insulators specifically polymers such as rubber, nylon, Teflon etc., but, it can also be observable in conductive materials. Triboelectrification is inevitable process of intimate contacts [7] which occurs at not only solid to solid interface but also solid-liquid [8] and solid-gas [9] interfaces. One of the other interesting nature of triboelectrification is that besides different materials, neutral identical materials are also charged oppositely when they are brought into contact and separated [10].

Triboelectricity is ubiquitous in environment even can be faced in daily life such as feeling discharge shock while touch somebody or material after walk on the carpet or rub wool, or funny experiments in elementary school where a paper

is rubbed to hair and after it sticks to balloon. Moreover, triboelectrification is also encountered frequently at industrial applications, especially in polymer powder included granular systems [11] and pharmaceutical product formations [12].

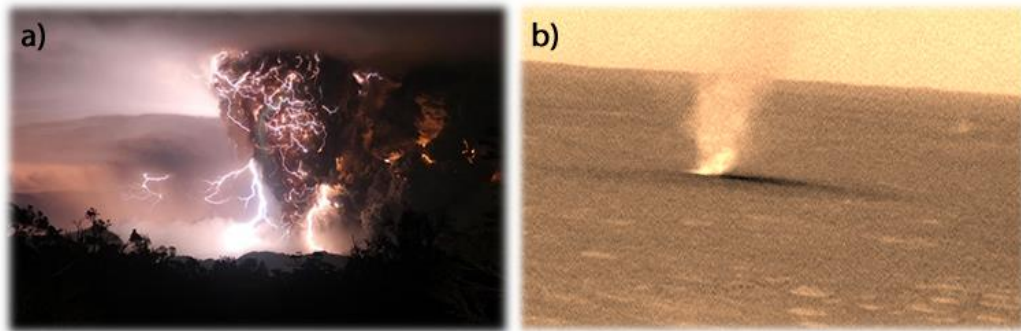


Figure 2.1: Triboelectrification in environment: (a) Volcanic lightning during Chaitin volcano eruption, 2008 [13]. (b) Dust devil on Mars is observed by Spirit rover, 2005 [14].

Triboelectrification can also be observable at natural phenomenon such as lightning during thunderstorm where movement of air layers produce ice crystals and soft hails that collide with each other results in triboelectric charge generation and following by high potential electrostatic discharges [15]. Dust devil and sand storms are another electrostatic charge carrier in which particles of sand are scattered by the wind blows cause triboelectrification of them occurs on Mars' surface as well [16,17]. Furthermore, in volcanic plumes, particles of ash collide with each other conclude in triboelectric charge generations following by volcanic spark discharges [18]. It is quite remarkable phenomenon claimed that chemical origin of life could originate from volcanic lightning which trigger several amino acid syntheses from mixture of various gases that has represented by Miller-Urey experiment [19].

2.2. Triboelectric Series

Early posteriori over triboelectrification is triboelectric series, firstly advanced by Wilcke in 1757 [20], in which different materials are listed with respect to their relative triboelectric polarity. In these series, various materials are placed into list

in the order of positive and negative charged materials near the top and bottom respectively where relative polarities are obtained by systematic contact electrification experiments. Later on, Faraday, Jamin and Bouty studied on empirical lists of triboelectric series in 19th century followed by Shaw, in 1917, who performed numerous experiment with using gold-leaf electroscope in order to obtain triboelectric series of elementary metals, various types of furs and woods, and other insulators [21]. Following, empirical studies related triboelectric series have been extended more as researchers include polymeric materials to their triboelectric series. In Table , four different qualitative triboelectric series in the literature is represented [22].

Regarding to detailed investigation of triboelectric series comparisons, although series are constructed by different laboratories, index or order of materials are quite similar except for small number of inconsistencies. Nature of contact process and surface variations of experimental setups are one of the main reasons for inconsistent measurements [23]. In other words, triboelectrification includes consecutive steps of contact and separation where it is very hard to arrange similar conditions in different measurements about contact pressures, surface impurities and oxides, magnitude of friction forces etc.

In order to minimize external affect, several quantitative methods have been developed to measure generated triboelectric charge densities in recent years. Inductive probes are essential technique to measure magnitude of tribocharge densities which are generated by laminar contact pairs and particles [24,25]. In this methods, probe is placed over source of triboelectric charges where electrostatic potential generate induce current on inductive probe. Solid state electrometers are frequently used devices to measure magnitude of induced charge density on electrodes which are either attached triboelectric source or surround sample of triboelectric charge source with faraday cup [26,27]. Furthermore, in recent years scanning probe techniques such as electrostatic force microscopy (EFM) and Kelvin probe force microscopy (KPFM) are used to investigate contact electrification process more precisely [28-31].

Table 2.1: Comparison of triboelectric series in different studies [22].

Ref. Coehn (1898)	Ref. Hersh (1955)	Ref. Henniker (1962)	Ref. Adams (1987)
Positive charge			
		Silicone elastomer with silica filler	Air
		Borosilicate glass, fire polished	Human hands
	Wool	Window glass	Asbestos
		Aniline-formol resin	Rabbit fur
		Polyformaldehyde	Glass
		<i>Polymethyl methacrylate</i>	Mica
		Etylcellulose	Human hair
		Polyamide 11	
Nylon 6,6	Nylon	Polyamide 6-6	Nylon
		Rock salt (NaCl)	Wool
		Melanime formol	Fur
		Wool, knitted	Lead
		Silica, fire polished	Silk
Cellulose	Viscose	Silk, woven	Aluminium
		Polyethylene glycol succinate	Paper
Cellulose acetate		Cellulose acetate	
		Polyethylene glycol adipate	
		Polydiallyl phthalate	
		Cellulose (regenerated) sponge	
	Cotton	Cotton, woven	Cotton
		Polyurethane elastomer	Steel
	Silk	Styrene-acrylonitrile copolymer	Wood
		Styrene-butadiene copolymer	Amber
	Acetate	Polystyrene	Sealing wax
Polymethyl methacrylate	Lucite	Polyisobutylene	Hard rubber
Polyacetate	Polyvinyl alcohol	Polyuretane flexible sponge	Nickel, Copper
	Dacron	Borosilicate glass, ground state	Brass, Silver
Polyethylene terephthalate		Polyethylene glycol terephthalate	Gold, Platinum
		Polyvinyl butyral	Sulfur
		Formo-phenolique, hardened	Acetate, Rayon
		Epoxide resin	Polyester
		Polychlorobutadiene	Styrene (Styrofoam)
	Orlon	Butadiene-acrylonitrile copolymer	Orlon
		Natural rubber	Saran
Polyacrylonitrile		Polyacrylonitrile	
<i>Polyvinyl chloride</i>	<i>Polyvinyl chloride</i>	Sulfur	
Polybisphenol carbonate	Dynel		
Polychloroether	Velon		Polyurethane
Polyvinylidene chloride			
Poly(2,6-dimethyl polyphenylene oxide)			
<i>Polystyrene</i>			
<i>Polyethylene</i>	<i>Polyethylene</i>	Polyethylene	Polyethylene
<i>Polypropylene</i>		Polydiphenyl propane carbonate	Polypropylene
		Chlorinated polyether	
		Polyvinyl chloride with 25% DOP	Vinyl (PVC)
		Polyvinyl chloride without plasticizer	Silicon
		Polytrifluoroethylenoethylene	
		Polytetrafluoroethylene	Teflon
Negative charge			

2.3. Theory of Triboelectricity

Even though, the picture of contact electrification including observations in daily life, industrial applications and natural phenomenon, and studies over empirical consistent triboelectric series is clear as conceptually, it is very hard to refer same about theory behind it. There has been ongoing research in widespread disciplines in which physicist, chemists, engineers and meteorologists strive to understand theory behind triboelectric charge generation, and yet clear-cut conclusion has not been appeared [32,33]. Heretofore, there have been mainly hypothesized three alternative mechanisms underlie triboelectric charge generation: Electron transfer, ion transfer and material transfer.

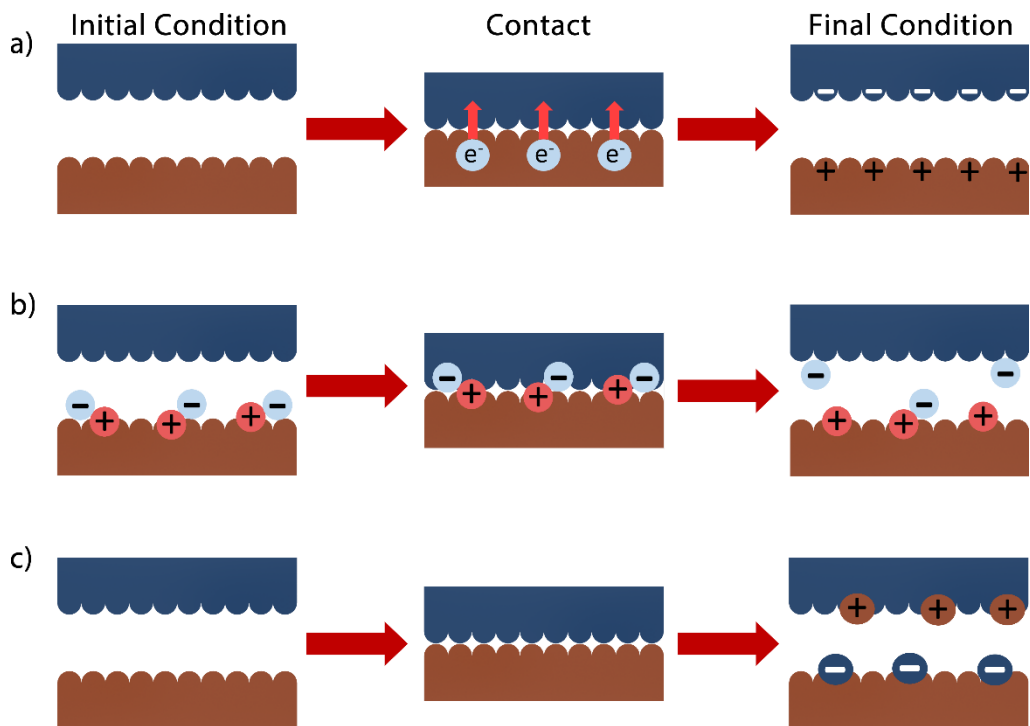


Figure 2.2: Schematics of the proposed triboelectrification mechanisms. (a) Electron transfer mechanism, in which electrons are exchanged due to different work functions of materials. (b) Ion transfer mechanism, strongly bounded fixed ions and mobile counter ions are represented as positive and negative polarities respectively, in which mobile ions are transferred after intimate contacts. (c) Material transfer mechanism, in which charge generation is originated from transferred material species.

2.3.1. Electron Transfer

The electron transfer mechanism primarily focus on conductor triboelectrification in which it is considered that electron exchange arises from difference in work function of conductors [34]. Work function ϕ is intrinsic feature of conductors defined as minimum thermodynamic work to extract an electron from the surface of solid. In case metals that have different work functions brought into contact, contact potential difference V_c would take place between metal surfaces results in tunneling of electrons e in order to maintain thermodynamic equilibrium [35]:

$$V_c = \frac{\phi_2 - \phi_1}{e} \quad (2.1)$$

Harper explored that parallel plate capacitor approach can be adapted to this mechanism in order to determine total amount of transferred charge [36]. Regarding to contact area and metal to metal separation distance based capacitance C_s of system, total amount of transferred charge Q can be obtained by:

$$Q = C_s V_c \quad (2.2)$$

As mentioned before, triboelectrification process involve both contact and separation steps, here contact step initiates charge transfer and separation step limits amount of charge transfer where tunneling of electrons is terminated above critical separation distance [36]. Thus far, metal-metal contact electrification is only phenomenon that researchers have common ground electron transfer is main reason for this type of triboelectrification.

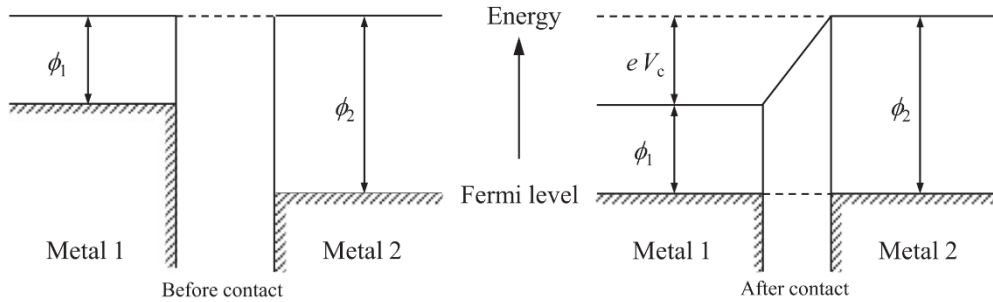


Figure 2.3: Electron transfer between metal-metal contact [37].

However, electron transfer approach which is results of work function differences cannot be implemented metal-insulator and insulator-insulator contacts directly, since insulators has huge band gap between valance and conduction bands, electrons cannot transfer between them [37]. In other words, considering intimate contacts of two different insulators I_1 and I_2 , valance band electrons of I_1 can transferred neither valance nor conductor band of I_2 , due to all valance states of I_2 are filled and electron cannot fulfill energy to terminate conductor band respectively.

In this case, regarding the metal-insulator and insulator-insulator contacts, researchers have considered to extend work function difference based electron transfer model with surface state theory [10,38]. Theory accounts insulator surfaces have specific surface state levels and corresponded effective work functions where electrons in different materials transferred between these states. Later on, Fabish and Duke renewed electron transfer model in insulator contacts with proposing acceptor and donor states for insulator surfaces [39]. However, both of electron transfer models about insulator-metal and insulator-insulator contacts still have been argued due to theoretical drawbacks and lack of experimental evidences [3,32].

2.3.2. Ion Transfer

In 1960s, development in electrophotography have revealed that polymeric toners that contain ionomers or molecular salts have also mobile ions on particle surfaces where in general, strongly bounded immobile ions and loosely bounded mobile counter ions take place with opposite polarities [5,40,41]. Thus, mobile ions can be transferred between different insulators when they are brought into contact would result in oppositely triboelectric charged insulators. In parallel to this theory, several experiments have performed with polymer to polymer contacts and polymer-metal contacts have demonstrated transferred ion concentrations [42,43].

However, ion exchange mechanism cannot be implanted to contact electrifications of nonionic polymers since they do not accommodate mobile ions. Following to this claim, it is proposed that hydroxide ions on the polymer surfaces can provide mobile ion necessity for ion exchange mechanism with regards to reports about humidity based hydroxide ion existence on polymer surfaces [5,43-45]. On the contrary, recent experiment done by Baytekin and colleagues have demonstrated that water is not compulsory for triboelectrification but it supports to balance surface charges [46], come into conflict with the claim that ion exchange is the only reason for contact electrification.

2.3.3. Material Transfer

The material transfer theory comprises that sub-micron scale pieces of materials are transferred from the surfaces of rubbed materials due to friction. These pieces presumably carry charges since transferred particles arise from either bond breaking process or contamination of surfaces [47]. However, it is argued that contact electrification is reproducible process therefore material transfer cannot be dominant factor in triboelectrification since its extent might be decreased at repetitive contacts [48].

Regarding to material transfer mechanism, in 2011, Baytekin and colleagues [29] performed systematic experiments and characterizations about contact electrification and have refuted long-held idea that surface are charged homogeneously opposite polarities after the intimate contact of materials. On the contrary, “mosaics” of both positive and negative charges at different quantities distributed at each surface lead positive or negative net charge distributions [29].

Furthermore, a detailed x-ray photoelectron spectroscopy analyses are performed by same group demonstrated presence of both charge and material transfer in contact electrification [30].

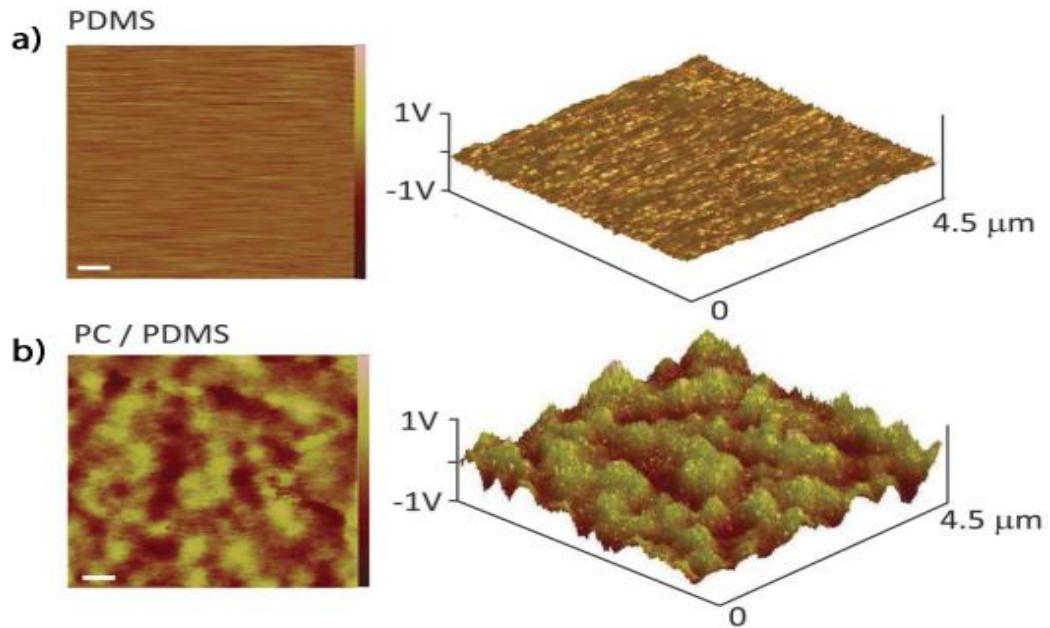


Figure 2.4: “Mosaics” of generated triboelectric charge potentials are scanned via KFM [29]. Polydimethylsiloxane (PDMS) surface potential maps (a) before contact, (b) after intimate contact with Polycarbonate (PC).

2.4. Applications of Triboelectricity and Triboelectric Nanogenerators

Contact electrification is inevitable phenomenon of mechanical contacts independent from conductive or insulator characteristics of materials. Although, there is not a lower limit for the amount of triboelectric charge generation, dielectric strength of atmosphere limits maximum generation of triboelectric charge density correspond to approximately $10^{-3} C/m^2$ in air [3,35]. In this point, several methods are demonstrated to either increase or decrease the generated triboelectric charge density depends on application type.

Triboelectrification is one of the important concern of electronic industry since possible electrostatic discharges (ESD) can be destructive for electronic components [49]. Furthermore, it can trigger flame or explosions at combustion gas or petroleum used industries. Therefore, it is crucial to control contact electrification

process in these industries. Following to this concerns, studies on recent years about de-electrification process [50] and development of the antistatic polymers [51] would yield to prevent unexpected electrostatic discharges due to contact electrification in ESD sensitive industry.

On the other hand, triboelectric charges are utilized at several applications electrostatic separation over the centuries. In early of twentieth century, Graaff invented electrostatic generator based on contact electrification of rubbed belt reaches very high electric potential have been used in particle acceleration applications [52]. Following years, triboelectric charges led to development of electro-photography through contact electrification based charged toners [53].

Electric field generated by triboelectric charges and coulomb interaction between charged particles makes triboelectrification feasible to be utilized in e, filtration and separation applications specifically in recycling industry [54] and electrostatic powder coating applications [55].

In recent years, with the advancement in nanotechnology, researcher have been enabling to control and manipulate triboelectric charges in micro-nano scale. In that direction, triboplasma has demonstrated which is generated by triboelectrification can be used in surface modification applications [56].

Furthermore, in 2012, Wang demonstrated triboelectric nanogenerator (TENG) as a new type nanogenerator that utilize triboelectrification of materials and electrostatic induction principle to generate electricity can be used as cost effective, sustainable and portable energy harvester or self-powered sensor [57], [58]. Since 2012, innovative developments on TENGs have been leading to establish correlation between triboelectrification and wide range application area and remarkable acceleration on triboelectricity research.

2.5. Operation Modes of Triboelectric Nanogenerators

TENGs convert mechanical energy to electricity have diverse application areas in general, macro or micro scale energy harvesting and self-powered sensors. In parallel to these applications, various types of configurations are designed in order to harvest energy by using triboelectrification of structural dielectrics as well as freely moving triboelectric sources in environment, mainly can be divided to four categories: Contact-separation mode, sliding mode, single electrode mode and free standing triboelectric layer mode.

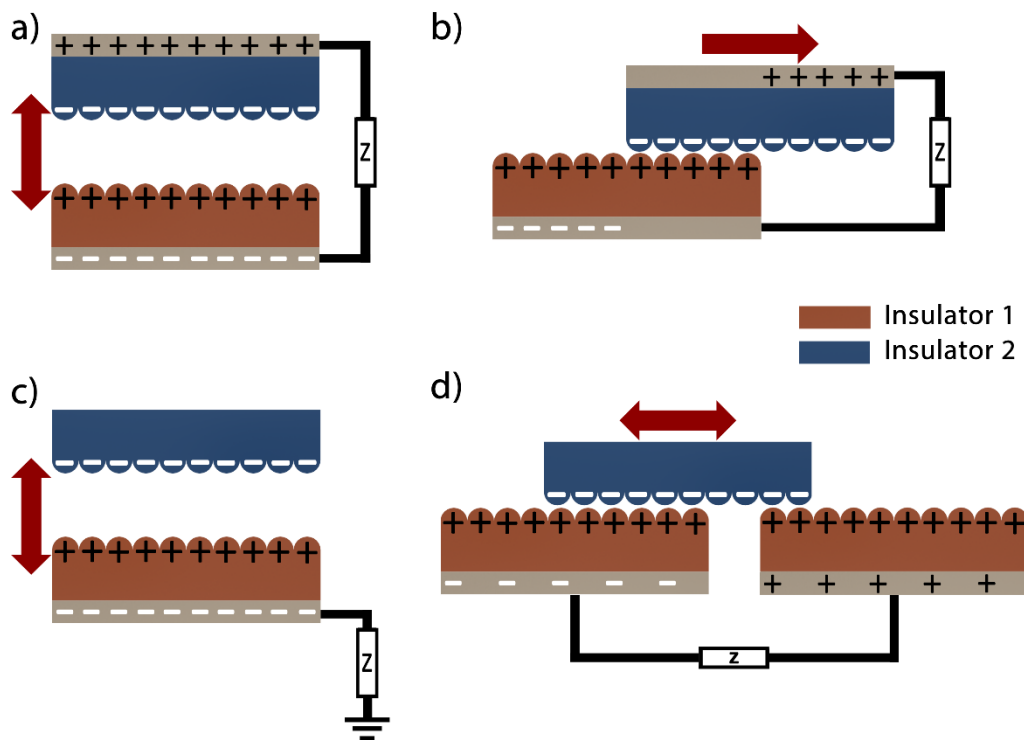


Figure 2.5: Schematics of TENG operation modes. (a) Contact-separation mode. (b) Sliding mode. (c) Single electrode mode. (d) Free standing triboelectric layer mode.

2.5.1. Contact-Separation Mode

The first fundamental triboelectric nanogenerator mode is vertical contact-separation in which layers of TENG are fabricated as sandwich type structure [59]. The working mechanism of vertical contact separation mode is illustrated in Figure 2.6. In this mode, once pre-separated dielectrics of TENG are brought into contact by the external mechanical force results in triboelectric charge generation on the surfaces of dielectrics. When layers are separated by a small gap, electrostatic potential difference is established between the two planar electrodes which are fixed on exterior faces of dielectrics. In case connection of electrodes with electrical load, free electrons in electrode near the negatively charged dielectric would flow in order to balance electrostatic field, overall called as electrostatic induction. If layers are pressed to original position by external force electrostatic potential would be lowered and vanish at the full contact ensue back flow of electrons. Eventually, repeating contact and separation steps generate alternating current through external electrical load in which frequency is formed by contact and separation cycle.

As mentioned before, triboelectric charges are generated between not only insulator-insulator contacts but also insulator-conductor contacts. Therefore, vertical contact separation mode can be formed with either double dielectric layers [60] or dielectric-conductor layers [61].

Vertical contact separation mode is simplest design of TENG consists of dielectric layers, electrodes and separation gap in a sandwich structure. Polymers are mostly used components as dielectric layers due to exterior triboelectrification characteristics specifically Teflon (PTFE) which is placed at the bottom of triboelectric series (Table 1). However in recent years, inorganic materials [62], chalcogenides [60] and liquids [63] are also used as triboelectric charge source.

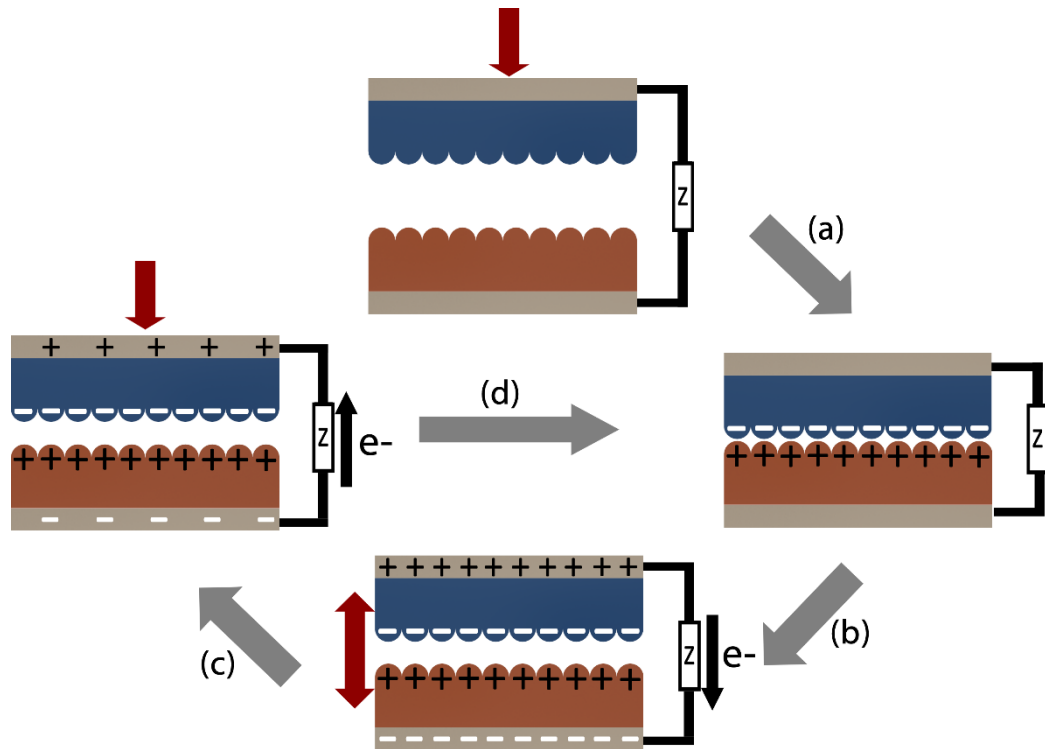


Figure 2.6: Working mechanism of contact-separation mode. (a) Pressing step in which external force brings the two insulators into contact, resulting in triboelectric charge generation on surfaces. (b) Releasing step leads induced electron flow between electrodes. (c) Re-pressing by external force leads electron backflow due to potential difference variation. (d) Intimate contact step is established again in which electron flow reaches equilibrium.

Electrodes act as free electron source in overall working mechanism of TENG can be integrated outer surfaces of dielectrics in various way. Deposition and coating are effective techniques provide closest integration to dielectrics, on the other hand adhesive aluminum tapes can also be used as electrode. Separation gap plays an crucial role in the working mechanism of contact-separated TENG mode usually sustained by springs which allows to self-releasing after pressing [61]. In addition curved structure are also used to provide simultaneous releasing for separation gap [59]. Furthermore, multi layered vertical contact separation mode based TENGs are formed by packing several TENG structure with the help of 3D printed supports [60] or in zigzag form in which many of TENG units attached each other from their edges [64].

2.5.2. Sliding Mode

In sliding mode, triboelectric layers constructed at complete contact state as represented in Figure 2.7. Unlike vertical contacts at previous mode, here lateral sliding leads generation of triboelectric charges. Therefore, triboelectrification occurs only aligned cross sections of surfaces. Regarding the working mechanism of sliding mode, at the beginning, there would be no potential drop due to absence of separation gap. Once, lateral separation of surfaces is driven by external force, surfaces, and hence charges are also separated lead electrostatic potential difference. Similar to vertical contact-separation mode induced current would flow between electrodes through external load resistance in order to balance initial electrostatic potential drop. Following, backward sliding would generate opposite directed current form alternating current in overall.

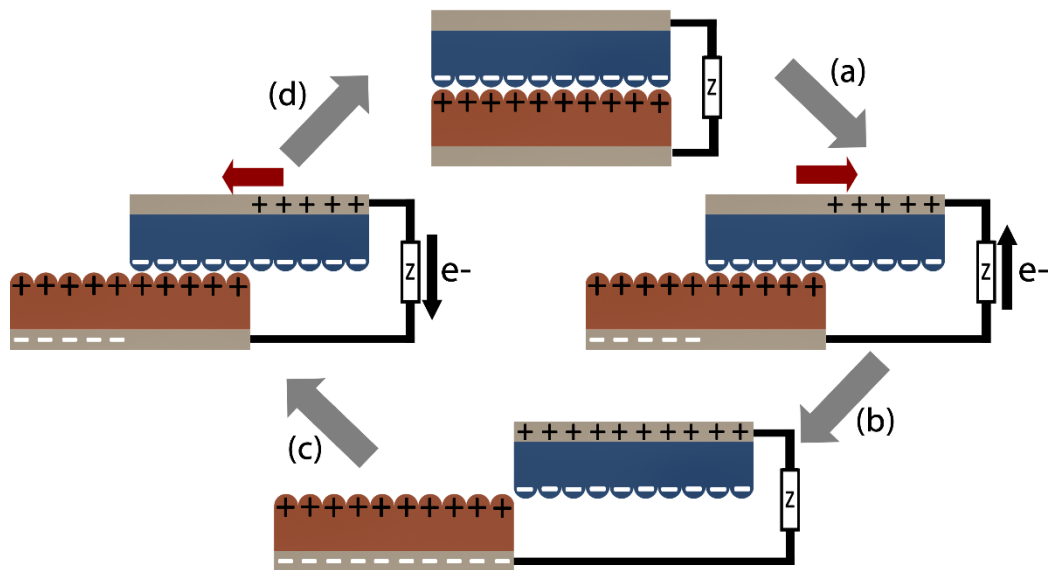


Figure 2.7: Working mechanism of sliding mode. (a) Lateral sliding via external force initiates induced electron flow. (b) Full separation of insulators results in electron flow saturation. (c) Backward sliding yields electron backflow to balance electrostatic potential drop. (d) Complete contact step in which electrostatic potential difference vanishes zero.

It can be claimed that in sliding mode, contact area is reduced at least at the begin and end of movement may diminish efficiency, however experiments assert the contrary because sliding yields more triboelectric charge generation with respect to plain contact [65]. The other advantageous of sliding mode is to be suitable for various types motions such as planar [66], circular [67,68] and rotational [69] with highest extent of flexibility.

2.5.3. Single Electrode Mode

As introduced before, triboelectrification is inevitable phenomenon of all of mechanical contacts in nature, and TENGs have capability to harvest energy by simply using this fact. However, the two modes mentioned above focus on triboelectrification only sustained by dielectrics inside a solid and compact designed device makes unable to use of triboelectric charges at environment. In this instance, single electrode mode was introduced to harvest energy by account freely moving arbitrary triboelectric charge sources at environment such as human skin [70], tires [71] and rain drop [72].

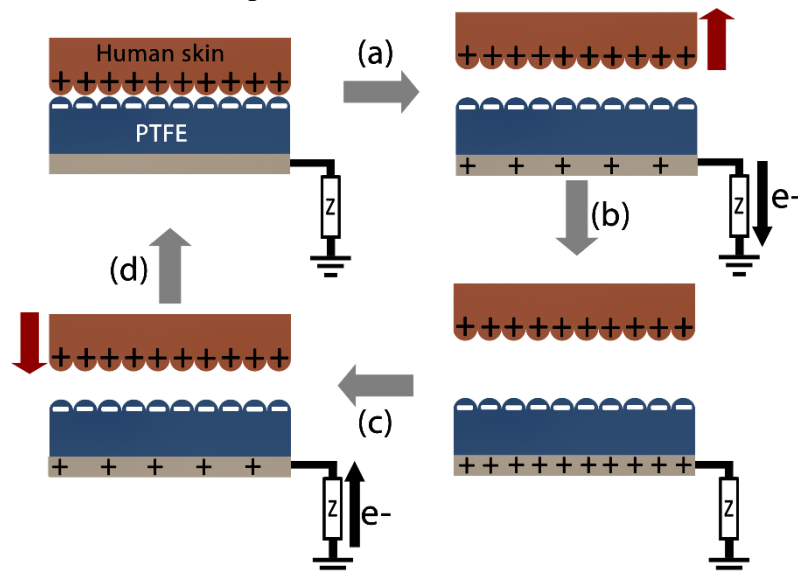


Figure 2.8: Working mechanism of single electrode mode. (a) Contact and separation of human skin generate electrostatic potential difference which yields electron flow through external load (b) When critical separation is supplied system comes into equilibrium. (c) While human skin coming closer to PTFE layer, electrostatic potential drop is emerged which results in backflow of electrons. (d) Complete contact condition is established again in which electron flow reaches equilibrium.

The energy harvesting by single electrode mode TENG can be equipped pairs of freely moving dielectric source and fixed either single electrode or dielectric layer attached electrode [73]. In case of dielectric layer attached electrode structure is represented at Figure 2.8. Human skin which is accounted as arbitrary dielectric source is coming into contact with fixed Polytetrafluoretilen (PTFE) layer where electrode is deposited outer surface of polyester has connection to ground. Once, vertical or sliding contact between dielectrics is established triboelectric charges with opposite polarities would be generated on surfaces. Contingent upon departure of human skin electric field difference would be produced which would yield free electron flow from electrode through ground until field variance is balanced, to be concluded as positive charging of electrode. Subsequently, coming closer of human skin through PTFE again would lead depreciation of electric field concluded by back flow of electrons from ground to electrode. Eventually, repeated touches and leaves of human skin to fixed polyester layer would generate electricity in alternating form which can be driven through external load placed between electrode and ground.

Regarding to comparison of single electrode mode with respect to dual electrode systems, efficiency in single electrode mode is lower than others due to the absence of second electrode which limits amount of generated charge by electrostatic induction process [74].

2.5.4. Free-Standing Triboelectric Layer Mode

Free-standing triboelectric layer mode TENGs are built as similar to single electrode systems, the only difference is placing at least one or more fixed triboelectric layer near present one [75]. Regarding to working mechanism of this mode, arbitrary freestanding triboelectric source comes into contact with fixed triboelectric layers which are separated among a certain gap distance. Once, contact and separation steps are proceeded between three of dielectrics along either vertical or lat-

eral motions, nonuniform triboelectric charge distributions, and hence electrostatic potential difference would be developed. Therefore, induced electrons would flow between electrodes lead current generation.

In free standing triboelectric layer design, fixed layers can include either electrode attached dielectrics or simple electrodes without dielectrics because both conductors and insulators exhibit triboelectric charge generation under mechanical contacts [76]. Furthermore, fixed triboelectric layers can be arranged following two configurations; side by side position where fixed layers underlie free standing layer [77] or vertically multi-layered position where free standing triboelectric layer is positioned between fixed layers [78]. A key advantageous of this mode is being capable to harvest energy from vibrations, large scale motions [79] and textile platforms [80] as well.

2.6. Fabrication and Characterization of Triboelectric Nanogenerators

Besides various operation modes in which a convenient one can be chosen with respect to application area, in general fabrication process including material selections and structure optimizations play a key role regarding to designation of operation efficiency of TENGs. As mentioned before, TENGs convert mechanical energy to electricity by using combination of triboelectrification and electrostatic induction. Regarding to electrostatic induction step, augmentation of induced charge population is essential factor to enhance energy harvesting efficiency. In this motivation, separation gap distances which can be either vertical or lateral depend on operation mode, and elapsed times means velocities between contact and separation steps are primary parameters of structural optimizations [81]. Furthermore, unique design of hybridizing TENG with electromagnetic generators have been reported in order to coupled effective charge generation from induced potential [82,83].

On the other hand, in contact electrification step, material selection, surface area and surface morphology are major factors in order to enhance amount of generated triboelectric charges.

The output power of TENGs is directly proportional to generated triboelectric charge densities, thus choosing best contact electrified dielectric pairs spontaneously assure efficiency enhancements. In parallel to this consideration, triboelectric series are convenient sources for material selections in which materials are listed in the order of relative polarizations during contact electrification process. Thus metals and nylon, and fluoropolymers such as PTFE, polyvinylidene fluoride (PVDF) and fluorinated ethylene propylene (FEP) are commonly used materials in TENGs as indexed at the top and bottom respectively in triboelectric series (Table 1). On the other hand, some of applications necessitate specific materials, for instance water and chemical liquids are used in hydropower energy harvesting [79] and self-powered chemical sensors [84] respectively. Additionally, utilization of transparent [85], recyclable [62], biodegradable [86], biocompatible [87] and self-healing [88] materials provide diverse application area for TENGs.

Besides the choose of intrinsically high order triboelectric materials, chemical surface functionalization processes are an alternative way to enhance triboelectricity of materials. Fluorination of surfaces by either fluorocarbon plasma treatment [89] or fluorine monolayer coating [60] are one of the effective ways to improve negative polarization affinity during contact electrification. Cation and anion injection is an alternative method to increase order of surface charge polarity results in enhancement on output power [90]. However, as mentioned before, maximum surface charge densities of dielectrics are limited by dielectric strength of ambient atmosphere where contact electrification is hosted, thus efforts in order to increase dielectric charge density lose its effectivity at some point. In this case, studies about ionized air injection over polymer surfaces have demonstrated that ionized gas molecules settle on polymer surfaces and lead to change dielectric strength of ambient atmosphere along their volume concentrations results in improvement on maximum limit of surface charge density [91].

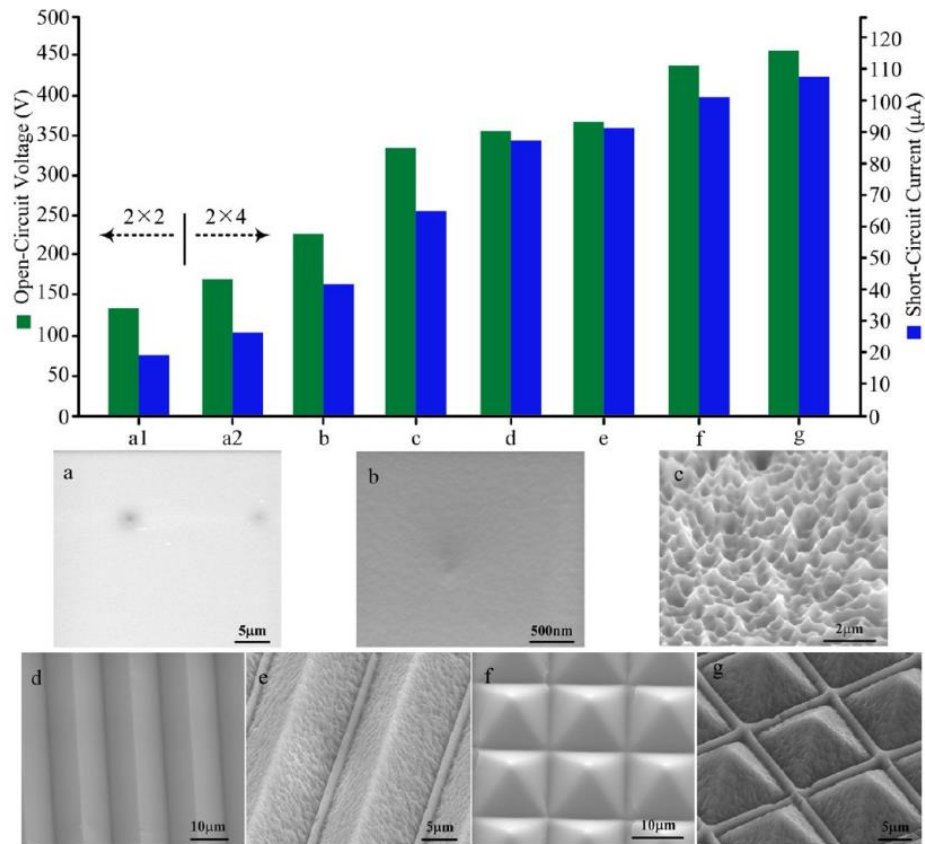


Figure 2.9: Effect of surface morphology on TENG output performance [98]. Scanning electron microscope images of (a) plain polyethylene terephthalate (PET) film, (b) plain PDMS film, (c-g) surface structured PDMS films.

Indeed, most important parameter has directly effect on output power characteristics of the TENGs is active surface area of triboelectric layers where intimate contacts are taken place [81]. Output current is linearly proportional to contact areas which can be increased by either roughly enlarging device dimension or multilayer designed structures [92]. On the other hand, changing surface morphology, rather device dimensions, by micro/nano surface modification techniques, is alternative way to enlarge contact area while conserve compactness and portability of device. In 2012, Xiao and colleagues have performed systematic fabrications and characterizations about surface structured TENGs, as it represented in Figure 2.9, surface morphology has remarkable importance on output power while material difference and device dimension affect output power slightly. There are

several studies about functionalization of triboelectric layer surfaces through grating structures [93], nanopillars[94], nanowires [95] and nanoparticles [96] demonstrate that increase of the surface roughness by these structures lead to enhance device energy conversion efficiency. In addition to nanostructure deposition over triboelectric layer surfaces, direct micro/nano fabrication techniques are also frequently used to enhance surface roughness of layers such as photolithography [97], soft lithography [98,99], block copolymer self-assembly [100,101], plasma etching [102,103], printed circuit board [104] and UV embossing [105].

2.7. Applications of Triboelectric Nanogenerators

Along fundamental operation modes, promising renewable, cost effective, sustainable and portable energy harvesting characteristic of TENGs lead to develop various type of applications can be categorized under four main group as large scale energy harvesting, mobile and portable harvesting, self-powered sensors and tribotronics.

2.7.1. Large Scale Energy Harvesting

Over past decades, rising energy need of technology and limitless of fossil energy sources lead to energy productions from renewable sources such as solar, hydro and wind by solar cells, dams and wind turbines respectively. In this motivation, TENGs are alternative promising candidates to harvest energy from these renewable sources either directly or in hybridized formation with conventional energy harvesters at macro-scale.

In 2013, the first hydropower based TENG is developed in the form of contact-separation mode consisting functionalized surface structured PDMS layer and water interference [63]. Following years, various type of prototypes; spherical [106], box [107], spring integrated [108] and duck-shaped [109] structures are developed through using either contact electrification of water flows such as rain drops and

ocean waves or kinetic energy of water fluctuations in rivers, oceans etc. In parallel to these developments, TENG networks [110] are demonstrated, by the combination of multi hydropower based prototypes, in order to large scale energy harvesting where estimates assert around 1MW electric power generation per kilometer square area [111].

Wind power is another alternative free energy source where researcher have been achieved to generate electricity from wind pressurize and oscillations through planar or rotational single electrode based flexible and textile structured TENGs [80,112] . On the other hand, advancement on thin and transparent electrode integration into TENGs such as indium tin oxide [113] and conductive nanoparticle deposited transparent polymers [114] yield possibility to hybridization of TENG units with other renewable energy harvesters such as wind turbines and solar cells [115]. Transparent TENG units are successfully integrated over solar cell surfaces in order to generate electricity from water drops in rainy days as well as winds in windy days [116].

Considering to, limitless wave and flow power of broad water distribution across earth, wind and rain drop sources as well, hybrid TENGs and TENG networks are would be promising candidate to harvest energy from these renewable power sources in the near future, if energy converting efficiency can be improved, structural robustness-sustainability of networks can be ensured, and sufficient energy storage-transfer mechanisms can be developed.

2.7.2. Mobile and Portable Energy Harvesting

Mobility and portability are certain characteristics of personal electronics such as cell phones, laptops, watches etc. However, battery which supplies limited energy source is the main problem along development of consumer electronics also obstruct miniaturization process. In this content, TENGs as being a sustainable, mobile and portable energy power source are integrated with small scale electronics

in several applications in order to either supply energy demand of electronics directly or charge preexisting batteries through energy harvesting from environment.

Applications of TENGs in small scale are mostly about biomechanical energy harvesting in which human motions [64,117,118], hand pressing [119] and even sounds [120] are utilized as mechanical and vibrational energy sources. Walking in which averagely 2J/step [121] is consumed for pressing to ground is a ubiquitous mechanical energy source for TENGs in order to convert this waste energy into electricity, accordingly many of shoe integrated TENG applications demonstrated in flexible formations [118,122]. Furthermore, development of completely transparent TENGs, and their integration over touchscreens-display units allows to harvest energy along consecutive finger touches through either contact electrification of human skin or contact pressure of touches [99,119].



Figure 2.10: Application areas of TENGs [170] . (a) TENG as a biomechanical energy harvester and power source for small scale electronics. (b) Energy harvesting from environment by TENGs and their promising application areas.

On the other hand, flexible textile based TENGs have attracted remarkable attention since integration of these structures into fabrics allows to generate electricity from clothes, carpets, curtains etc. Although, conventional TENG fabrication techniques are inadequate to produce textile platforms directly, several applications are demonstrated by either integration of flexible traditional triboelectric layers with commercial fabrics [80,123,124] or woven structured dielectric yarns and electrode-coated or inherent conductive yarns [125-127].

Beside biomechanical energy, other vibration and motion sources in daily life such as cars, engines and even furniture are utilized in small scale energy harvesting applications of TENGs [60,61]. Furthermore, TENGs and other types of nanogenerators, piezoelectric and pyroelectric, are hybridized to operate as sustainable and efficient power source in consumer electronics through harvesting both mechanical and thermal energies from ambient environment [128,129].

2.7.3. Self-Powered Sensors

Indeed most powerful application area of TENGs is self-powered sensors including motional and vibrational detections, and chemical identifications [130]. As mentioned before, output power characteristics of TENGs varies with respect to contact pressure. Once suitable calibration is applied, TENGs can be operated as vibrational and motional sensor in which output signal would be intrinsically generated by itself means self-powered. Moreover, regarding to single electrode and free standing triboelectric layer operation modes, amount of generated electricity strongly depends on both active surface contact area and triboelectric characteristics of freely moving source materials. Therefore, these modes can be used as both motional and material detections through shift in contact surface areas and materials triboelectrifications. In parallel to these unique sensor potential of TENGs, various type of self-powered mechanical energy differentiation based sensor applications are demonstrated in the forms of either single TENG unit or array structured multiple TENG units.

Self-powered sensing of biomechanical motions or vibrations are essential sensor application types of TENGs. In this regard, several applications are demonstrated in order to detect trajectory of body motions [131] and tactile map of finger touches [132,133], and also biomedical monitoring of breath and hearth rates [134-136]. Furthermore, recent developments of elastomer based transparent and flexible TENG structures lead to promising self-powered electronic skin applications of TENGs [137,138].

Beside of biomechanical, motional and vibrational change of objects in environment can also be sensed by TENGs. Accordingly, speed detection and displacement mapping of moving objects [139-142], pressure quantification of loads [58,143], speed and direction detection of wind [112,144], and sensing of acoustic vibrations [103] are successfully demonstrated by using various type of structured and optimized TENG units. Moreover, by using triboelectrification and flow fluctuations of fluid materials, self-powered chemical sensors are presented such as mercury ion detection [145], ethanol sensor [146], liquid and gas flow detection in capillary microfluidic systems [147] and dopamine detection [148].

2.7.4. Tribotronics

Besides energy harvesting and self-powered sensor applications, a signal generated by TENG can also be used to trigger semiconductor charge transportation as being the gate voltage source called as tribotronics which has a promising potential in robotics and human-machine interaction [149]. The concept of tribotronic is firstly emerged in 2014, by Wang's group who achieved to modify field effect transistor structure with additional contact electrified layer as a gate potential source resulted in external force controllable charge transportation, has named as "contact electrification field effect transistor (CE-FET)" [150].

Later on, several types of transistor structures are coupled with triboelectrification lead to develop mechanically controllable tribotronic logic circuits [151], phototransistors [152] and light emitting diodes [153].

Chapter 3

High Performance and Large Area Biomechanical Energy Harvesting Floor Tiles

3.1. Introduction

Energy is the most vital component of the life. Biological substances in the nature including animals, plants, reptiles and single cell organisms, are capable to convert and store energy from many different sources such as sun, water and food. Animals find that source of energy useful to travel distances and mobilization for finding more energy sources. Their body converts most of the intake energy into heat and mechanical motion during these activities. This energy cycle of the nature seems very complex and based on basic instincts. Nevertheless, evolution of the civilization drives mankind to find more energy sources. For instance, human consumes more chemical energy than the minimal requirements of the body. The extra energy either stored or converted in heat and motions. These extra movements and the heat generated during human motion activity can be classified as dissipated energy and can be scavenged using smart energy harvesting systems.

Although, this technology was seemed unachievable along several decades, recently, it became very promising after the development of low energy requiring mobile devices and high power output triboelectric nanogenerators (TENG) [154]. In this study, vertical contact-separation operation mode TENG is utilized in order to develop high performance and large area biomechanical energy harvesting floor tiles. To our knowledge, use of carbonblack polyethylene film as a high performance triboelectric layer and mass producible, low-cost Ar plasma surface modification technique have been first time demonstrated in TENG research. Accordingly, 1.52 mA and 5.4 kV peak to peak current and voltage values were obtained and achieved to power up to 1400 commercial LEDs by large area TENG floor tiles.

3.2. Effects of Device Structure and Material Properties on Output Performance of Triboelectric Nanogenerators

Triboelectricity, which is also called as contact electrification, have known for more than a century. There are several hypotheses about triboelectric charge generation, however, the basic physics underneath of this effect still was not understood perfectly. Beyond these discussions, researchers were able to facilitate this effect through converting mechanical energy to electricity by TENGs in which contact electrification and electrostatic induction phenomena between two surfaces of dielectrics and their relative movements are utilized to harvest energy. Several conditions should be considered before designing a TENG such as device structure, triboelectric polarity of dielectrics and surface properties of triboelectric layers.

3.2.1. Working Mechanism of Contact Separation Mode

Along to working mechanism of vertical contact separation mode TENG, electrostatic potential difference, charge transfer and separation gap distance lead theoretical equations, in overall denominated as “V-Q-x relationship” [155 , 156].

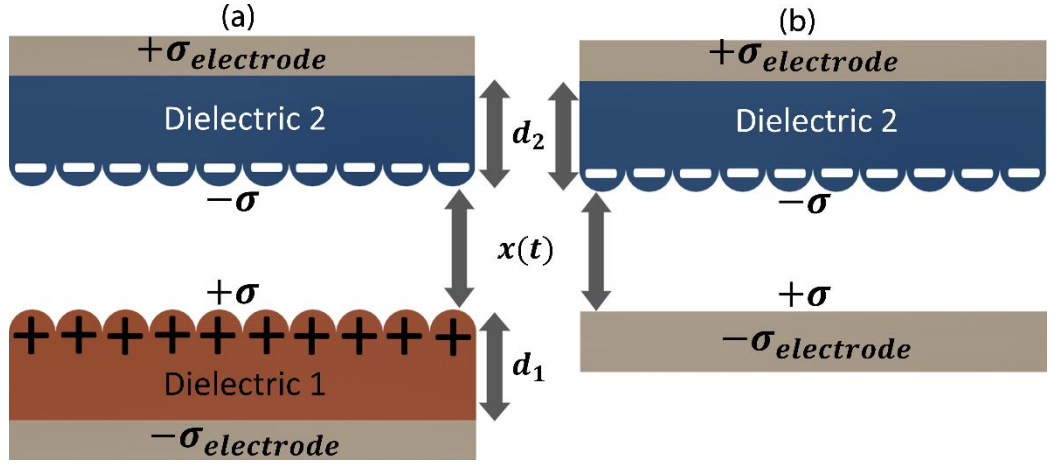


Figure 11: Vertical contact separation mode TENG device structures. (a) Dielectric-dielectric layered. (b) Metal-dielectric layered.

As stated in Chapter 2, vertical contact separation mode can be constituted as in the form of either double dielectric layers or dielectric-metal layers. In case of double dielectric layers assuming dielectric thicknesses d_1 and d_2 , dielectric constants ϵ_1 and ϵ_2 respectively, while contact step is established by external force, triboelectrification would lead opposite but equal charged surfaces with density of σ . Regarding to time dependent separation gap distance $x(t)$ electrostatic potential difference V can be given as;

$$V = E_1 d_1 + E_2 d_2 + E_{gap} x(t) \quad (3.1)$$

Where E_1 , E_2 and E_{gap} denote electric field strengths at inside dielectric layers and separation gap respectively can be derived by considering electrostatic induction which would yield opposite but equal induced charges at electrodes with density of $\sigma_{electrode}$, and using Gauss' law of charge on surface plate;

$$E_1 = \frac{-\sigma_{electrode}}{\epsilon_0 \epsilon_1} \quad (3.2)$$

$$E_2 = -\frac{\sigma_{electrode}}{\epsilon_0 \epsilon_2} \quad (3.3)$$

$$E_{gap} = \frac{\sigma - \sigma_{electrode}}{\epsilon_0} \quad (3.4)$$

Regarding to induced charge density equalization to total transferred charge Q divided by contact area A , Equation 3.1 can be reproduced as;

$$V = -\frac{Q}{A\varepsilon_0\varepsilon_1}d_1 - \frac{Q}{A\varepsilon_0\varepsilon_2}d_2 + \frac{\sigma - \frac{Q}{A}}{\varepsilon_0}x(t) \quad (3.5)$$

$$V = -\frac{Q}{A\varepsilon_0}\left(\frac{d_1}{\varepsilon_1} + \frac{d_2}{\varepsilon_2} + x(t)\right) + \frac{\sigma x(t)}{\varepsilon_0} \quad (3.6)$$

For the case of metal-dielectric triboelectric layers, absence of first dielectric would yield generation of both triboelectric charge (σA) and induced charge amount ($-\sigma_{electrode}A$) on metal layer end up with net charge of $(A\sigma - Q)$. In this case, the term E_1d_1 would vanish to zero because related dielectric replaced with conductor. Thus electrostatic potential difference would be;

$$V = -\frac{Q}{A\varepsilon_0}\left(\frac{d_2}{\varepsilon_2} + x(t)\right) + \frac{\sigma x(t)}{\varepsilon_0} \quad (3.7)$$

Regarding circuit characteristics of TENG, open-circuit condition (OC), and short-circuit condition (SC) would be investigated as considering absence of charge transfer at OC ($Q_{OC} = 0$) and electrostatic potential difference ($V_{SC} = 0$) at SC yield following equations (Equations are derived only for the dielectric-dielectric layered TENG for the simplicity, considering to dielectric-metal layers, the term d_1/ε_1 should be eliminated from following equations;

$$V_{OC} = \frac{\sigma x(t)}{\varepsilon_0} \quad (3.8)$$

$$Q_{SC} = \frac{A\sigma x(t)}{\frac{d_1}{\varepsilon_1} + \frac{d_2}{\varepsilon_2} + x(t)} \quad (3.9)$$

$$I_{SC} = \frac{dQ_{SC}}{dt} = \frac{A\sigma\left(\frac{d_1}{\varepsilon_1} + \frac{d_2}{\varepsilon_2}\right)v(t)}{\left(\frac{d_1}{\varepsilon_1} + \frac{d_2}{\varepsilon_2} + x(t)\right)^2} \quad (3.10)$$

On closer inspection to current characteristics of TENG at Equation 3.10, contact electrification active surface area and velocity of pressing-releasing cycle are key factors in order to enhance amount of output current while separation gap distance act on contrary.

Except charges on the surface of dielectrics, overall structure can act as parallel plate capacitor. Considering magnitude of charge stored on electrode Q and capacitance of system which is depend on separation gap $C(x)$, negative potential difference would yield as $-Q/C(x)$. Subtracting a potential differences of parallel plate capacitor and separated triboelectric layers $V_{oc}(x)$ results in net potential difference as;

$$V = -\frac{Q}{C(x)} + V_{oc}(x) \quad (3.11)$$

In this case, under short circuit condition of TENG, capacitance can be derived as equalizing potential difference V to zero and substituting Equation 3.8 and Equation 3.9 into Equation 3.11;

$$V_{sc} = 0 = -\frac{Q_{sc}}{C(x)} + V_{oc}(x) \quad (3.12)$$

$$C = \frac{A\epsilon_0}{\frac{d_1}{\epsilon_1} + \frac{d_2}{\epsilon_2} + x(t)} \quad (3.13)$$

3.2.2. Optimization of Surface Modification Technique

Theoretical derivations demonstrate that amount of generated triboelectric charges and contact area of triboelectric layers are key parameters of output power. Contact area of triboelectric layers can be increased by either roughly enlarging device dimensions or enhancing surface roughness of dielectric layers through surface modification techniques.

To investigate effect of surface structures on output power of TENG, firstly nanopillar surface structured polymer films were fabricated by melt infiltration

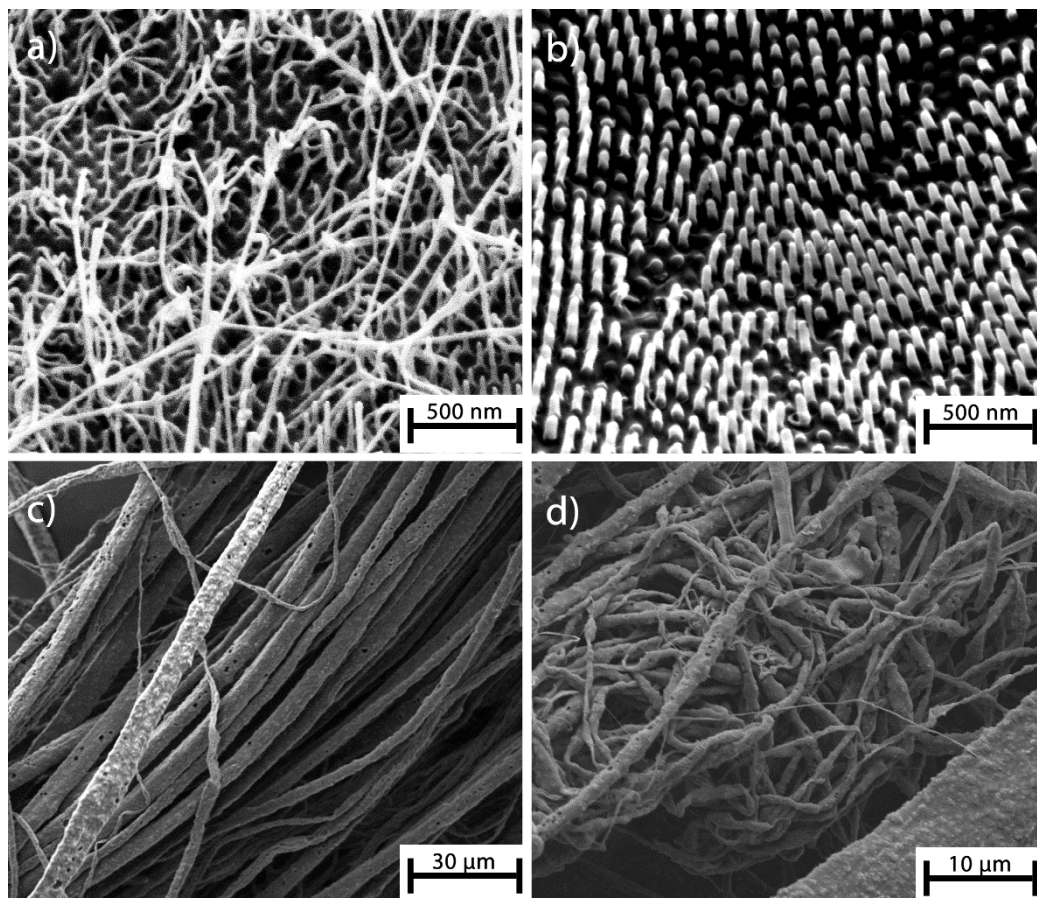


Figure 12: SEM micrographs of (a) PC nanopillars fabricated by AAO mold (b) PC nanopillars fabricated by Si mold (c-d) step-2 micro/nano CPE wires.

technique [157]. Once polymers are dissolved by chemical solvents, they introduce infiltration properties. When, liquid polymer solution is transferred onto anodized aluminum oxide (AAO) or silicon (Si) molds, which have nanostructured pores, polymer solution infiltrates into pores. Following, solvent is evaporated and solid polymer film is scraped from mold results in nanopillar surface structured polymer film. Accordingly, polyetherimide (PC) nanopillar structured films, PC (AAO) and PC (Si) were fabricated through using AAO and Si molds respectively. Scanning electron microscope (SEM) characterization of fabricated nanopillars are represented at Figure 12. Bottom fronts of the flat PC film, PC (AAO) and PC (Si) were coated with gold-palladium alloys as an electrode.

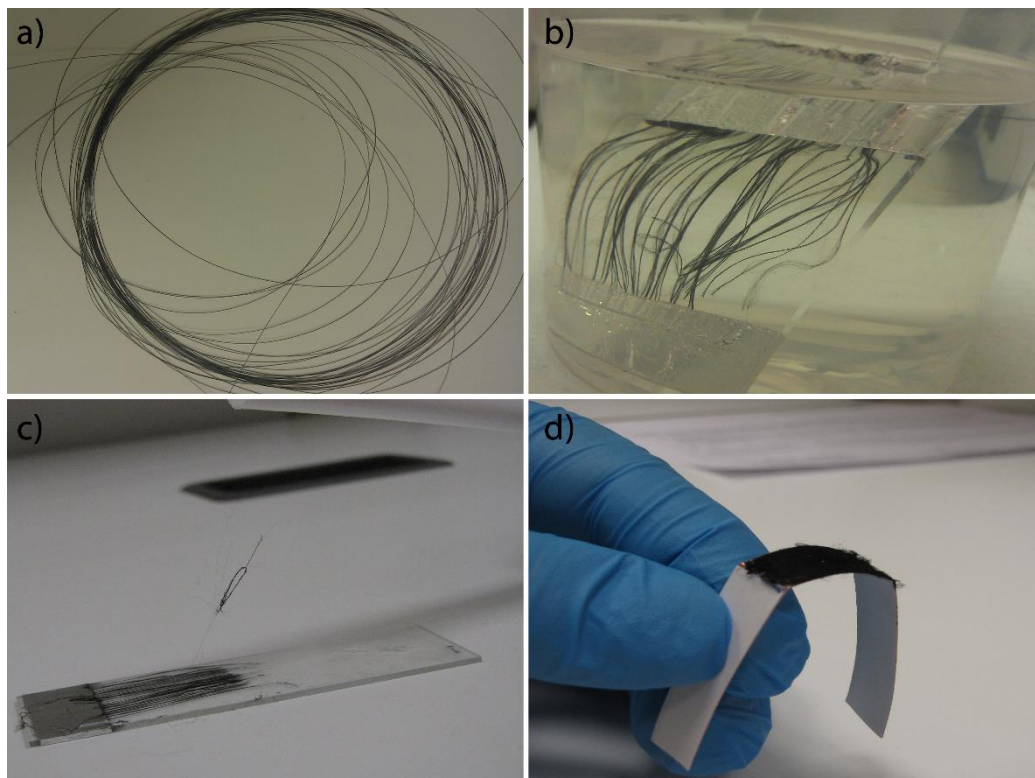


Figure 13: Step-2 CPE micro-nano wire preparation. (a) Step-2 CPE-PC/PSU core-shell fibers. (b) Chemical etching of fibers. (c) Electrostatic interaction of etched CPE micro-nanowires with PTFE rod. (d) Step-2 CPE micro-nano wire triboelectric layer.

On the other hand, iterative size reduction thermally fiber drawing, which is a novel top-down micro/nano fabrication technique, was utilized to fabricate carbonblack polyethylene (CPE) micro-nano dual scaled wires (detailed instruction of fiber drawing is given Chapter 4). Dichloromethane (DCM) was used for chemically selective etching fibers resulted in isolated CPE micro-nano dual scale wires which were transferred onto copper tapes, as an electrode, to construct triboelectric layers for TENG.

Finally, fabricated triboelectric layers were attached to thin flexible metal plates where plates were used to sustain self-releasing after contact step carried by tapping machine. Current and voltage measurements were performed with 5Hz tapping frequency. Output performances of different surface structured TENGs are represented at Figure 14 in which output power of TENG is dramatically increased as highest amount is obtained by PC (Si)-CPE (Step 2) micro-nano wire triboelectric layers.

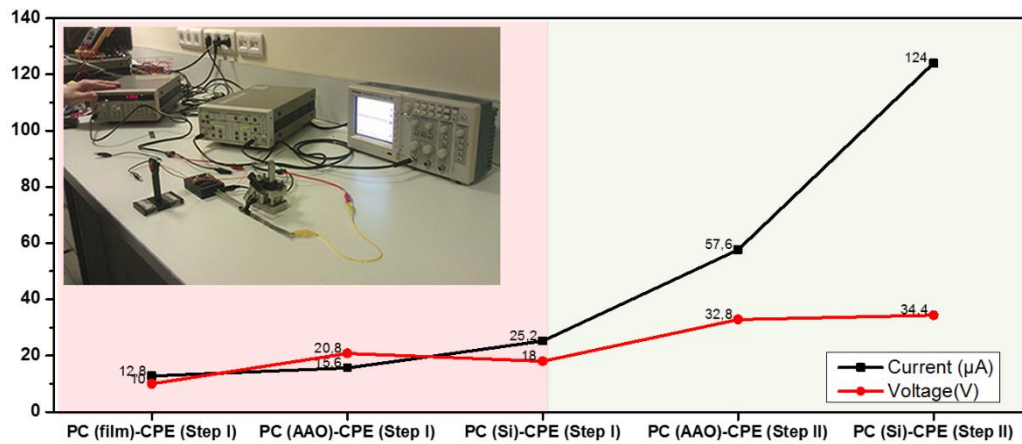


Figure 14: Output characteristics of different surface structured TENGs and current-voltage measurement system.

Nanostructured tribo-surfaces tends to generate more charges because the greater contact area is resulting with increased in amount of contact electrification. TENGs with simple and cost effective production processes were aroused at the historic moment. However, it is very hard to large area and cost effective mass fabrication of TENGs with using conventional micro/ nano fabrication techniques such as soft lithography [98,99], printed circuit board [104] and melt infiltration technique as our primary investigation. Therefore, these efforts should be carried on by introducing new aspects and proposing simple, efficient and cheap techniques.

Indeed, current study demonstrates an interesting fabrication technique, which is applicable to wide range of materials, using argon (Ar) plasma surface modification for manufacturing very high performance, low cost, mass producible, flexible and large area TENG devices. Essentially, plasma based surface modification is the interaction of the excited species (Ar, O₂, N₂, H₂ etc.) with a material, polymers in our cases. The plasma process depending on characteristics of material surface, excited species and also operation environment results in a physical and chemical modification of surface. While plasma surface modification, the plasma-generated excited species treat morphology, roughness and polymer chain structure of sample surface. Therefore, plasma surface modification technique provides greater contact area of polymer layers with large scale and mass predictability properties particularly for PTFE, which is hard to be surface structured by

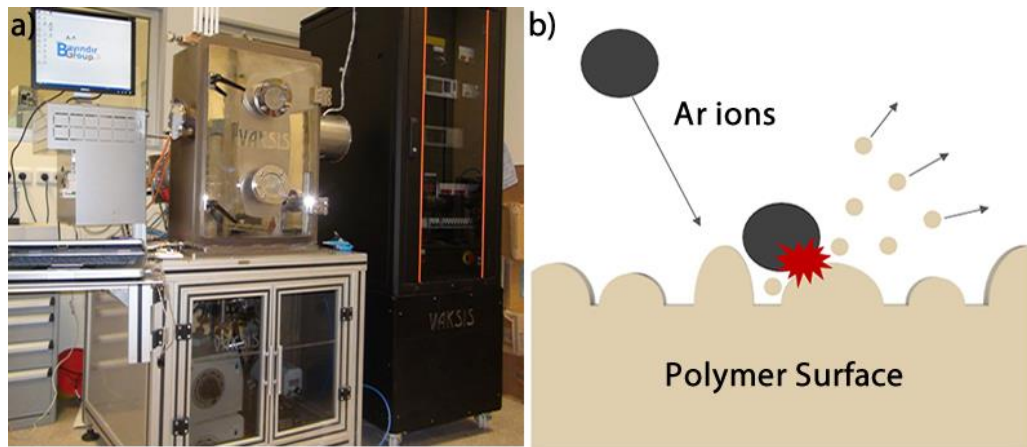


Figure 15: Argon plasma surface modification system and mechanism (a) Microwave sourced vacuum chamber (b) Schematic of Ar ions collision with polymer surface.

conventional techniques due to its high thermal and chemical stability. To investigate Ar plasma surface modification on TENG, a simple proof of principle device is constructed with PTFE and CPE films and remarkable increase on output power is obtained (detailed surface treatment and device output characterizations is instructed following section).

3.3. Fabrication of Large Area Triboelectric Nanogenerator Floor Tiles

Systematic material selection and surface roughness optimization by Ar plasma surface modifications were performed to construct high performance, large area biomechanical energy harvester.

3.3.1. Material Selections and Surface Treatment Optimizations

Triboelectric nanogenerators harvest mechanical energy into electricity through by utilizing contact electrification and electrostatic induction. Regarding to contact electrification step, order of generated triboelectric charge density is directly proportional to output current as stated in Equation 3.10. Charge generation is related indexes of materials in triboelectric series in which materials are

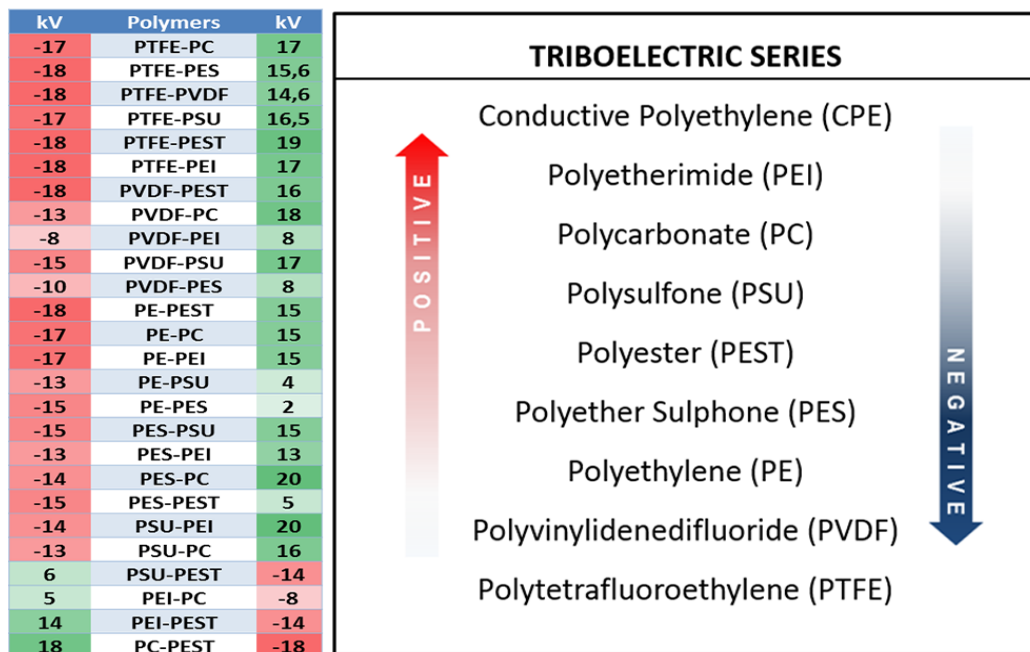


Figure 16: Triboelectric series constructed through relative electrostatic potential measurement by electrostatic fieldmeter.

aligned with respect to their relative charge polarities during contact electrification [22]. The greater span of two materials in series results with greater charge polarization during intimate contacts. However, materials sometimes represent different triboelectric characteristics rather than their position in triboelectric series due to surface impurities and contaminations based on industrial productions. Thus, in order to determine materials which will be used in large area TENG fabrication, triboelectric series of materials were obtained through electrostatic fieldmeter. As represented in Figure 16, polymers were systematically rubbed each other and their relative electrostatic surface potentials were measured by Simco FMX-003 electrostatic fieldmeter (CPE potential measurement are not represented since it gave zero electrostatic potential after each contact due to its conductive properties of).

First observation of triboelectric series investigations have demonstrated that PTFE and CPE films can be used in fabrication of high performance TENG. However, it should be considered that Ar plasma surface modifies not only surface morphology of polymers but also chemical properties such as polymer chain

structure, bond breaking etc. Therefore, materials can act on contrary as they indexed in triboelectric series after Ar plasma treatment. In parallel to this consideration, we optimized plasma surface nano-structuring mechanism for many different polymers, and built proof of principle TENG devices and compared their output powers in order to further detailed material selection.

All the polymers were modified in a custom made plasma chamber in which two roll of 30 cm in width and 80 cm in length polymer can fit. Ar plasma surface modification works as mechanical surface erosion using energetic Ar ions which has high molecular weight and chemically inert property makes enable to treat surface of polymers without changing bulk properties. Since different polymers

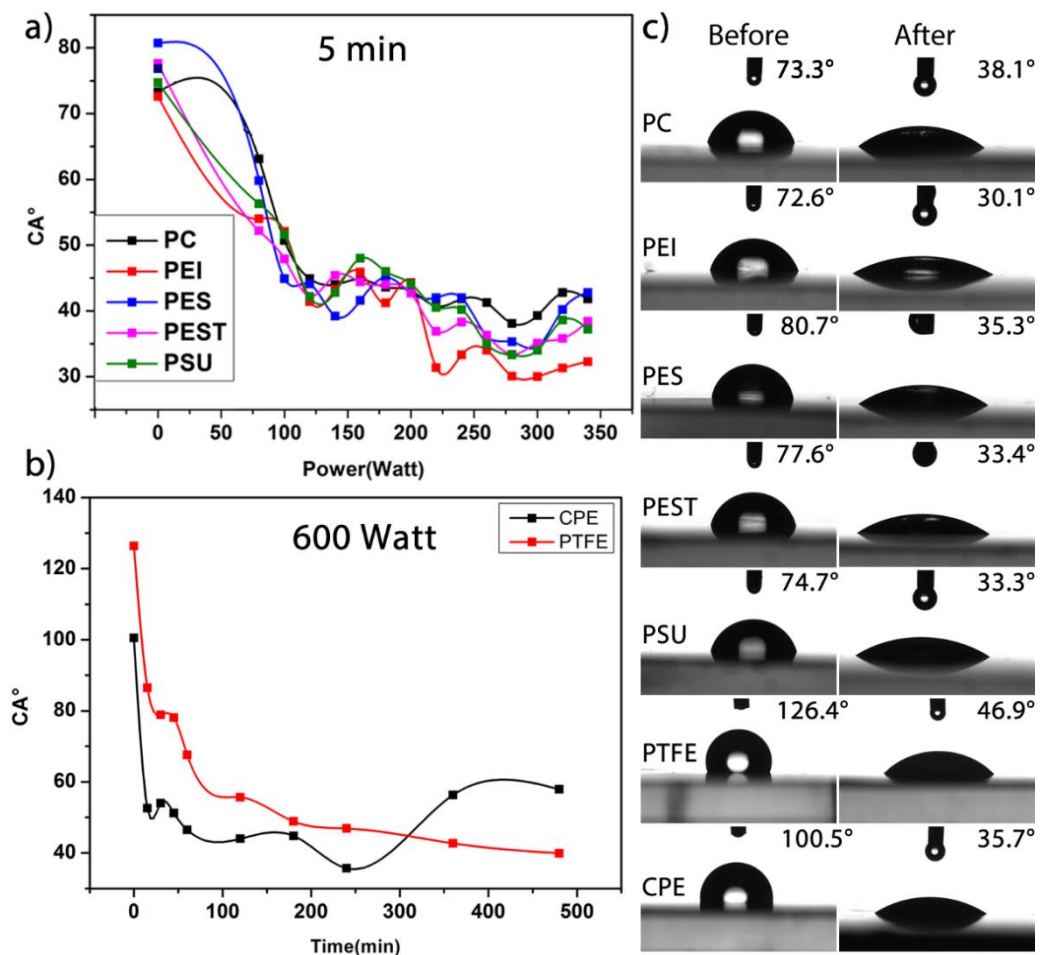


Figure 17: Ar plasma surface treatment optimization of (a) PC, PEI, PES, PEST, PSU, (b) CPE and PTFE films. (c) Contact angle images of polymer surfaces before and after plasma surface modifications, 5 min and 240 W for PC, PEI, PES, PEST, PSU films and 240 min, 600 W for CPE and PTFE films.

present different mechanical properties due to their molecular structure and chemical content, each polymer required specific plasma process parameters to obtain nano peaks on their surfaces. Chamber pressure, amount of the Ar flow and temperature were kept constant during all plasma processes. Only parameters that required to be tuned was process time and plasma power. At the low pressure (2.1 mTorr), 2.4 GHz microwave source is used to plasma treatment of polymer films. Computer specified power (80W-800W) were applied with magnetron under the Ar excess at 50 sccm to create Ar plasma. Polymer samples were introduced into the chamber with a special cylindrical holder in 7cm diameter and 28cm length which was rotated at 6 rpm. The distance between the polymer sample and the plasma source exciter was about 150 mm.

Surface nanostructures were also used to obtain hydrophilic microfluidic channels. Therefore, primary indication of surface nanostructures was the dramatic decrease in contact angles (CA) measurements which is the simple way to optimize surface roughness [158,159]. Contact angle goniometer measures contact angle between sessile drop and solid surface which gives information about energy of interface. Utilizing contact angle measurement technique, we optimized reacting power and reacting time of Ar-plasma to obtain lowest degree of contact angle since it directly relates about roughness of surface. As the roughness of surfaces increase, degree of contact angle decreases because of hydrophilic properties of surfaces. Accordingly, we measured contact angle of modified polymer surfaces which are treated in in different reaction times (0-480min) and reaction powers (80W-800W). Critical reaction time for PC, PEI, PES, PEST, PSU have obtained 5 min after 5,10,15,30 min operations. On the other hand, it was investigated that CPE and PTFE films need much more power and reaction time due to their chemical structures.

As shown in Figure 17, best wettability reacting power and time have been obtained as 240 Watt and 5 min respectively for PC, PEI, PES, PEST, PSU films and 240 min, 600 W for CPE and PTFE films. Following that, we characterized the surfaces of polymers using atomic force microscopy (AFM) operated in non-contact mode. Results were perfectly produced nano peaks within range 5 – 100

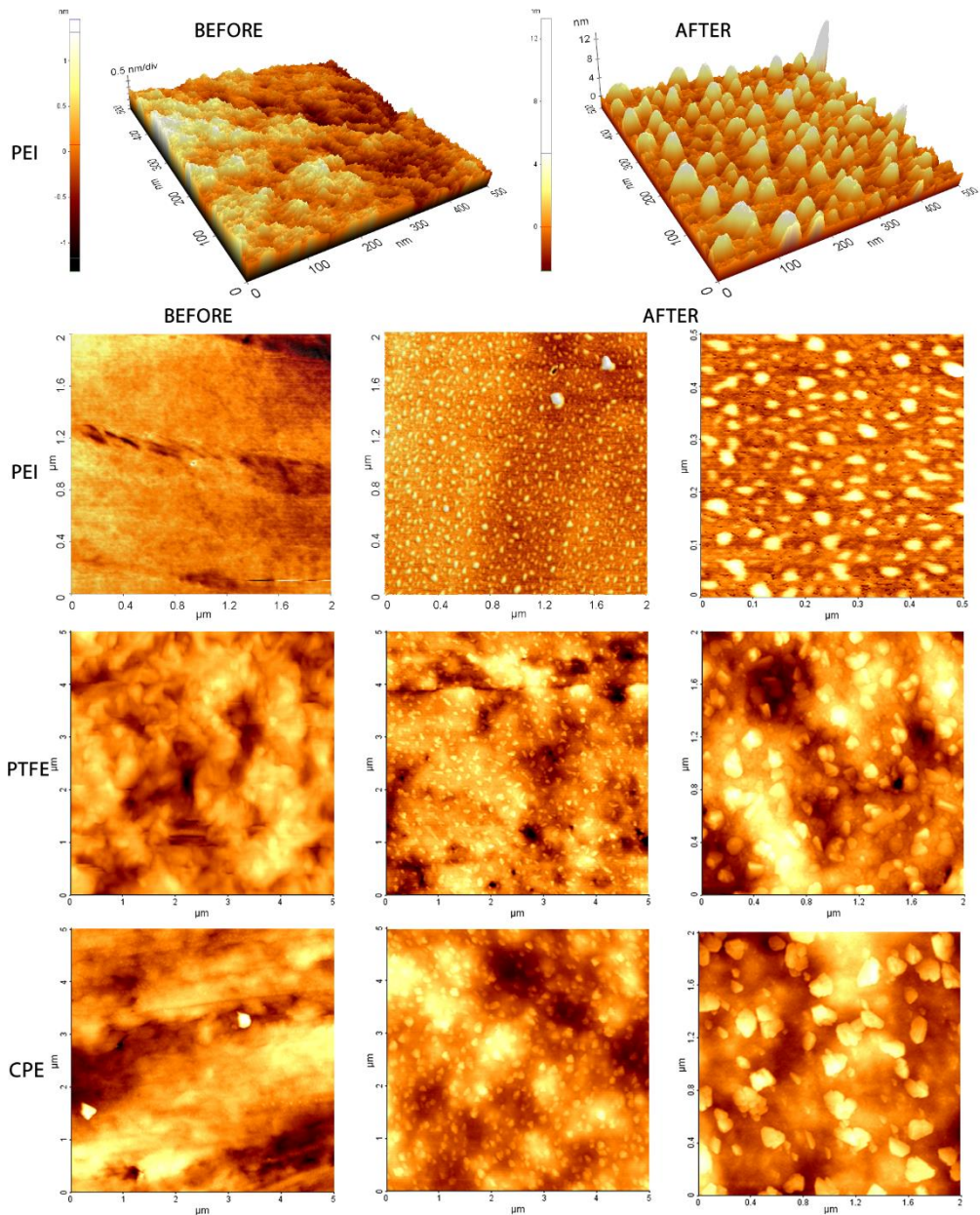


Figure 18: AFM images of polymer surfaces before and after plasma surface treatment process.

nm in diameter and length. In Figure 18, AFM images of PEI, PTFE and CPE film surfaces before and after plasma treatment at optimized reaction power and time are represented. As a result, effect of Ar plasma treatment process on surface morphologies of polymer films have been investigated and plasma modification reaction powers and durations have been optimized for each polymer as obtaining best surface roughness.

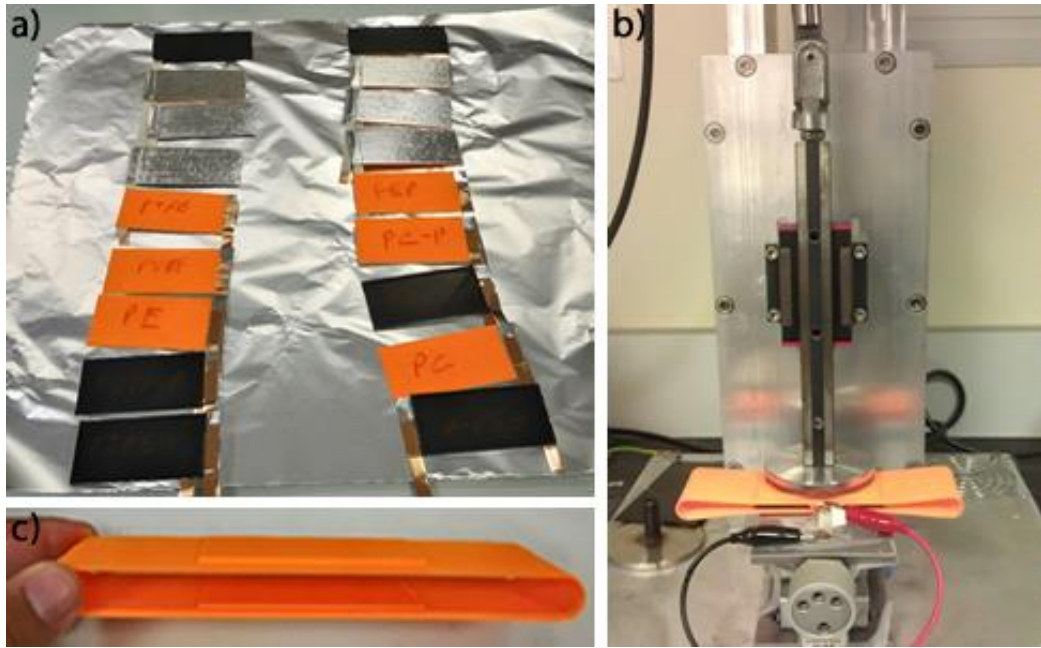


Figure 19: Fabrication and characterizations of miniature TENGs. (a) Preparation of triboelectric layers of TENG. (b) Custom made tapping device. (c) 3D printed TENG construction device.

Accordingly, we built many of miniature TENGs with listed polymers in order to investigate effect of Ar plasma surface modification on TENG output performances and come to a result of material selection for large area device. Polymers were paired and each pair was tested in a 3D printed construction in vertical contact-separation mode, which recently proven to be a simple and fast TENG fabrication method [60]. Identical size samples were tested at 5 Hz under same load sustained by custom made tapping device. Systematic measurements were resulted with highest output power of PTFE-CPE pair which can be also expected from triboelectric series and surface optimization for this pair results in further enhancement in output performance (Figure 20).

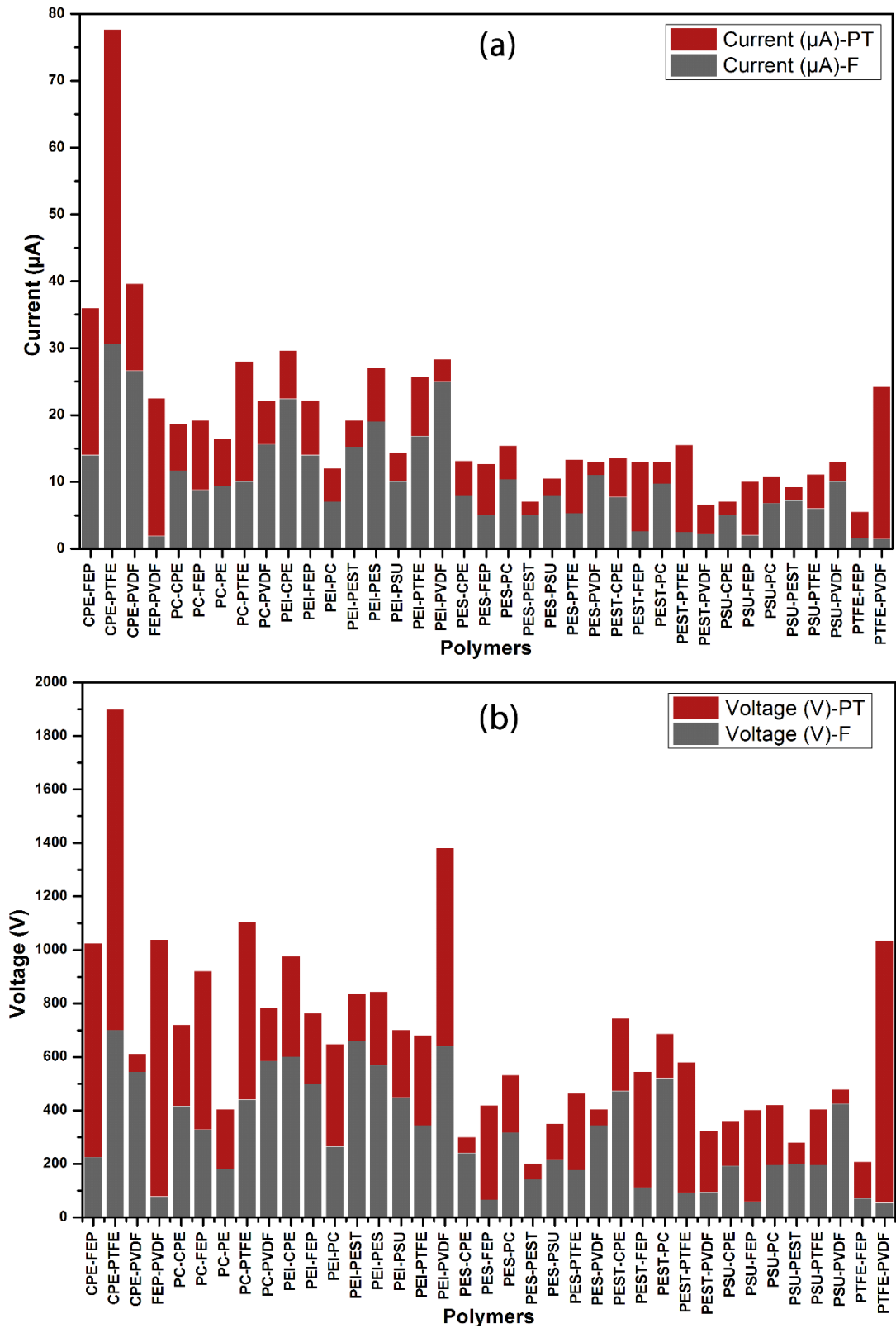


Figure 20: Output performance comparisons of flat polymer films (output-F) and Ar plasma surface treated polymer films (output-PT) based TENGs. (a) Short circuit current measurement results. (b) Open circuit voltage measurements.

Behind the material selection, these experiments open further investigations regarding to effect of plasma surface modification on materials triboelectric properties. To illustrate, PVDF is one of the most electronegative polymer in terms of triboelectrification polarization, it can also be confirmed from flat film based TENG output performances of it where has very low output current when it paired another strongly negative polarized polymer PTFE whereas as it expected it gave huge output with PEI which is placed towards positive side of triboelectric series. However, as it can be investigated from Figure 20, triboelectric characteristics of PVDF was totally changed after plasma treatment process whereas it gave huge output current with PTFE on the contrary low output current with PEI which means that Ar plasma surface treatment leads to shift triboelectrification polarity of PVDF from negative to positive side.

3.3.2. Device Structure

Systematic fabrication and characterization steps were successfully performed in order to choose triboelectrically high efficient material pairs resulted in choice of PTFE and CPE polymers. PTFE due to be lowest indexed material in most of triboelectric series, mostly used material in TENG research. On the other hand, to our knowledge, CPE have firstly used in this study where promising high performance triboelectric characteristics of CPE has been revealed for TENG research. Indeed, there are several reason for choice of CPE which are related about triboelectrification performance and its role in device working mechanism.

First of all, unlike most of polymer CPE has electrically conductive properties due to carbon doped chemical structure of itself. Besides the triboelectricity of material, charge transport efficiency within polymer itself and transferring efficiency of these charges from polymer to electrode also affect output current in TENGs. Polymers are usually considered as insulating materials because of their low conductivity. Most of polymers have low dielectric loss which allows them to store charges. Correspondingly, electrical conduction in polymers strongly depends on the transport of storage charges within the molecule itself and intermolecular

transport [58]. However, due to cross-link structures of polymers, interaction between polymer chains are weak and it causes low efficiency charge transport. Therefore, charge transfer between polymer particles and metal plates of electrodes is mostly arisen from electrostatic induction. In this limitation, in order to exceed direct charge transfer limit of conventional polymers, we have preferred conductive polymer as the CPE to generate higher power from TENG. CPE is carbonblack filled form of polyethylene(PE). Although, PE is insulator material as many of polymers, CPE has conductive property because of its carbon black(CB) filled structures which has similar to disordered graphite [160]. Regarding to some chemical or thermal processes, CB particle are filled into polymer matrices. Basically, filling CB particles form continuous conductive path in polymer as soon as concentration of CB particle reaching critical value which is called as percolation threshold [161]. Owing to, continuous conductive path of CB particles, polymers gain conductive property with saving organic structure, flexibility and triboelectrification properties. For this reason, we have chosen CPE as the counter pair of PTFE which act as both triboelectrification source and induced charge carrier due to its conductive properties.

Accordingly, PTFE and CPE polymer films in 18 cm x 18 cm dimensions were exposed Ar plasma surface treatment at optimized power and durations 600 W and 240 min respectively. After that, aluminum deposition was performed to non-treated side of PTFE film as an electrode by thermal evaporation system. Due to conductive properties of CPE film, we did not use extra electrode layer for it.

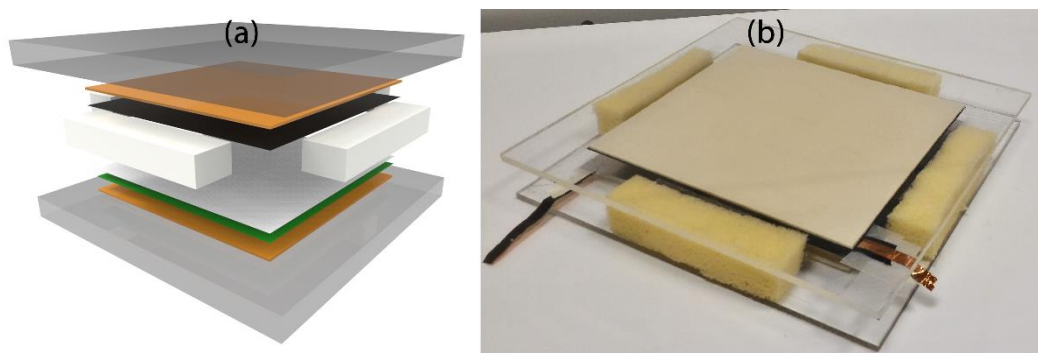


Figure 21: Large area TENG floor tiles. (a) 3D sketch of device structure. (b) Fabricated proof of principle device.

Following that, both of triboelectric layers were attached rubber as a support layer which prevents undesirable damages of strong vertical forces to triboelectric layer by assisting soft balance. Small pieces of thin copper tapes were stuck to electrode and directly to CPE layer in order to transfer induced charges towards external load. Later on, these triboelectric layers and supports were integrated with rigid acrylic plates to hold layers all together in vertical contact separation operation mode. Finally, relatively stiff foam pieces were positioned between the edges of acrylic plates to sustain self-releasing asi in spring assisted systems after pressing step which is implemented by external force.

3.4. Characterization

Based on the optimized fabrication parameters, we developed a proof of principle large area biomechanical energy harvesting TENG floor tiles. In Figure 22, detailed working mechanism of device is represented.

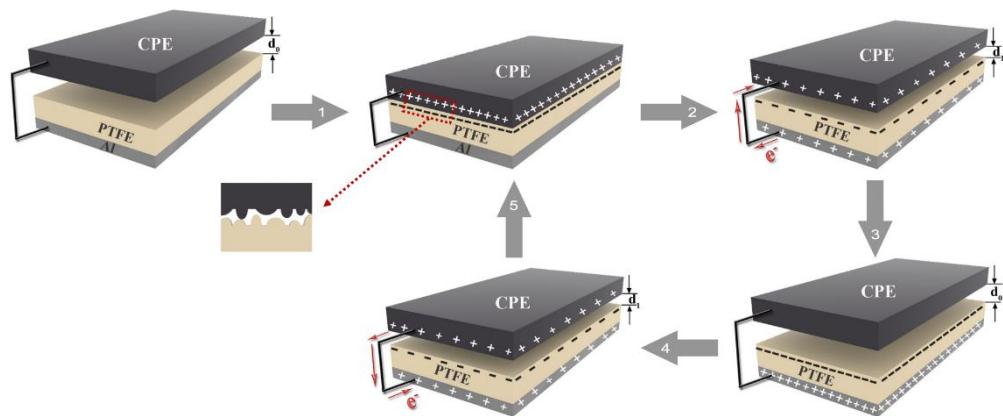


Figure 22: Working mechanism of energy harvesting floor tiles. (1) Initial contact step triggered by external mechanical source in which triboelectric charge generation takes place, (2) Self-separation of triboelectric layers when external force leaves results in electrostatic induction between conductive polymer and electrode, (3) Induced charges come into equilibrium at full separation, (4) Re-pressing over floor tiles leads electrostatic potential differentiation, and hence backflow of induced charges are initiated, (5) When separation gap distance vanishes to zero which also means full contact state, induced charge flow comes into equilibrium.

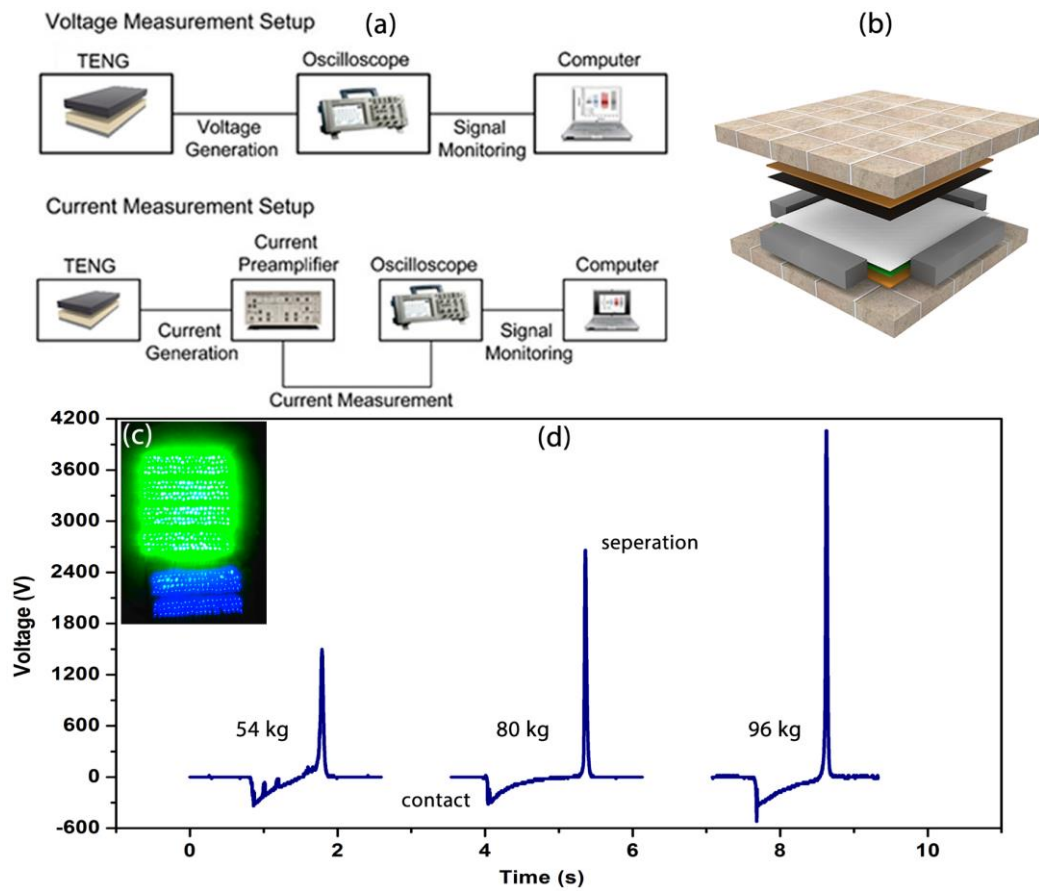


Figure 23: Output characterization of device. (a) Schematics of voltage and current measurement setups. (b) 3D sketch of TENG floor tiles. (c) Hand press over device instantaneously powered 600 green and blue LED. (d) Open circuit output voltages generated by TENG under single footsteps with different weighted biomechanical loads.

Output performance of device was characterized with respect to power generated by TENG under external forces of custom made tapping machine and biomechanical energy sources. Short circuit current and open circuit voltage measurements were performed through Tektronix TDS-1012B Oscilloscope and Stanford SR-570 Current Preamplifier, detailed setup is represented at Figure 23 (a). The device performance was firstly investigated with instantaneously powering 600 commercial green and blue LEDs through hand slaps and up to number of 1400 at 7 Hz constant frequency by using tapping machine. Later on, systematic current and voltage measurements were conducted by custom made tapping machine, which is capable to sustain adjustable tapping frequencies.

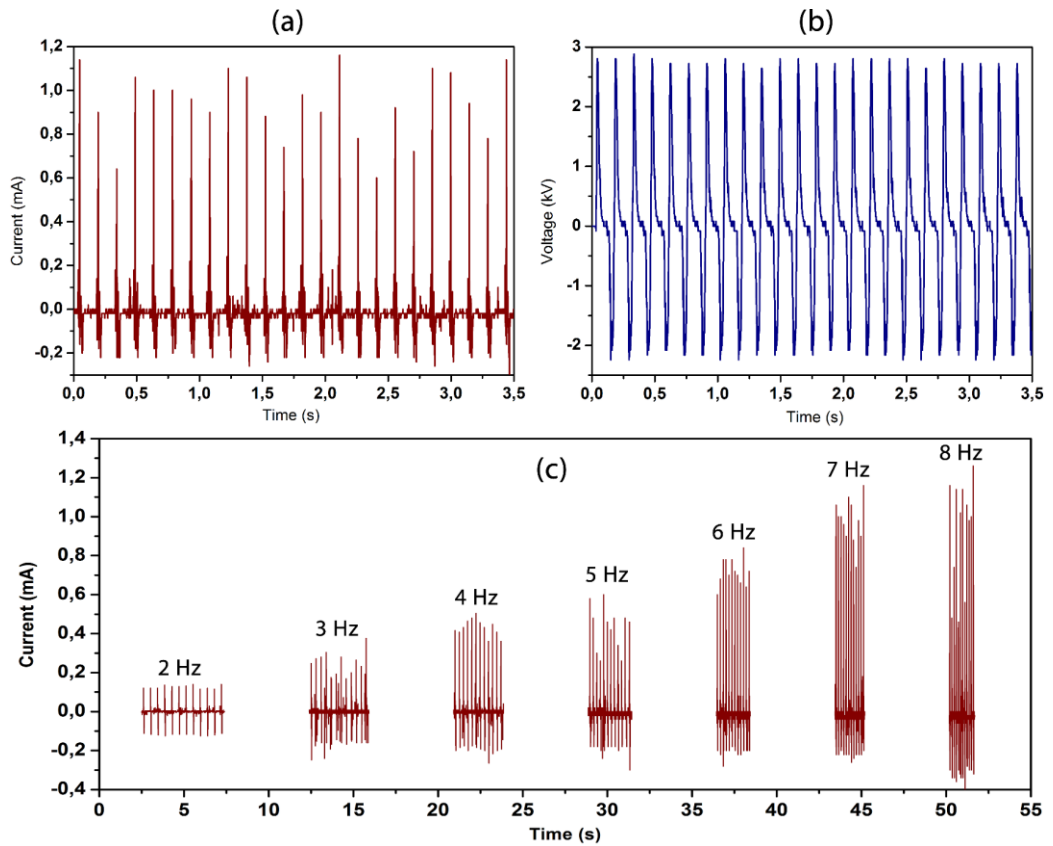


Figure 24: Output performance of TENG floor tiles. (a) Short circuit current and (b) open circuit voltage measurement at 7 Hz tapping frequency. (d) Frequency dependent output currents (2-8 Hz).

Maximum output current and voltage was obtained at 7 Hz tapping frequency as 1.52 mA and 5.4 kV peak to peak values respectively. Measurements conducted at different frequencies were indicated remarkable frequency dependence on output characteristics of device as represented in Figure 24 (c), output current of device rises as the tapping frequency increase up to 8Hz.

The output characteristics of TENG floor tiles were investigated also according to different biomechanical loads. It was observed that increasing the operator mass helps to harvest more energy. Furthermore, correlation between external load mass and generated open circuit voltage was demonstrated as represented in Figure 23 (d), output voltage is remarkably changing with respect to biomechanical load which demonstrates that besides the energy harvesting, TENG floor tiles can also be used as self-powered mechanical load or motion sensor if detailed calibrations and are conducted.

Chapter 4

Triboelectric Nanogenerator Fabrics

4.1. Introduction

Wearable electronics have attracted remarkable attention in the past years. Flexible batteries, smart electronics, biomedical monitoring devices and electronic skins are particular applications of textile based electronics [162-165]. In parallel to these applications, TENGs have gained to be part of wearable electronics family by their promising mobile and portable biomechanical energy harvesting and self-powered sensor capabilities, and hence textile based TENGs fabrication and application research have accelerated last years along several innovative applications [123-127]. However, conventional TENG fabrications mostly depended on lithographic polymer film based structures in which although high ordered flexible structures can be produced, film structure based approach makes inadequate to produce textile structures directly. Therefore, studies focus on either integration of conventional TENG structures with commercial fabrics or fabricating of textile TENGs by modification of fabrics with electrode coating or deposition which actually restraint practicality of devices.

Accordingly, in this study, we offer new fabrication perspective for production of TENG fabrics directly with ‘triboelectric nanogenerator fibers’. Indeed, triboelectric generators are consisting of surface contacted polymers as a triboelectric charge sources and metal electrodes as a current source by harvesting induced potentials of triboelectric charges. Here, we utilized thermally fiber draw technique to fabricate self-triboelectric nanogenerator fibers in formation of electrode core-polymer shell structure and developed proof of principle textile TENG.

4.2. Fabrication of Triboelectric Nanogenerator Fibers

Fabrication of triboelectric TENG fabrics was conducted in two step, fiber drawing and surface modification of drawn fibers. Accordingly, a proof of principle textile TENG was fabricated in woven structure with step-1 CPE-PC fibers and PTFE tape.

4.2.1. Fiber Drawing

Thermally fiber drawing is performed to fabricate TENG fibers which is a unique technique to produce polymer fibers at micro scale and nano scale as well with novel iterative size reduction technique [166]. In this technique, polymer films are rolled over a solid rod tube called as preform to be consolidated in thermal oven or consolidator in other words. Consolidation is a vacuum atmosphere thermal

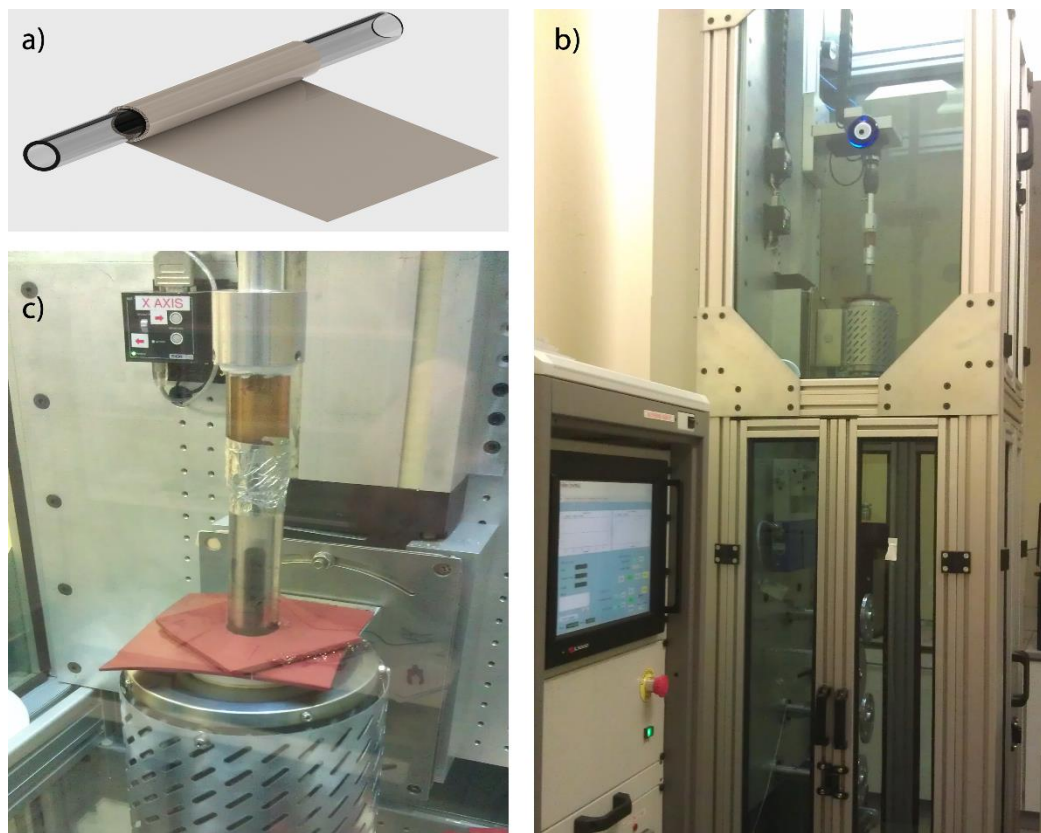


Figure 4.1: Thermal fiber drawing process. (a) Polymer film rolling over high melting point rod. (b) Custom made fiber drawing tower. (c) Preform is placed into furnace by preform holder.

process in which preforms are heated above their glass transition temperature results in tempered monolithic polymer rod. Later on, consolidated preforms are placed into fiber tower as represented at Figure (b-c) in which preform is driven into furnace with motion controllable preform holder. After that, thermal fiber drawing process is initiated with controlled heating of furnace. Furnace temperature should be above glass transition temperature but at the same time below the melting temperature of polymer, indeed previous empirical studies guide the optimum temperature. As a result, under high thermal stress phase of polymer rod is subjected to change means that fiber drawing is come into account. Laser micrometer and external controllable tensile force are utilized to real-time management of drawn fiber diameter. The unique property of thermal polymer driving is to produce multi-material core-shell fibers by rolling and consolidating polymer film altogether [167]–[169].

Utilizing thermal fiber driving technique, firstly we produced conductive polymer-insulator core-shell structured CPE-PC fibers. Initially, PC films were

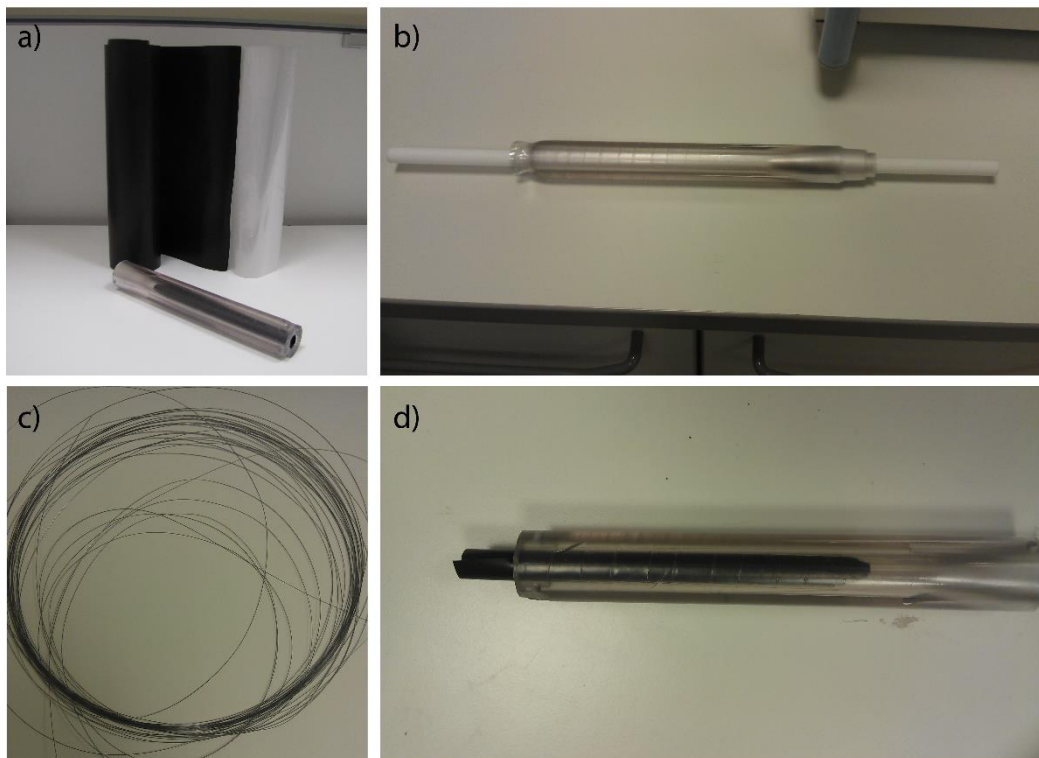


Figure 4.2: CPE-PC fiber drawing. (a) CPE and PC films. (b) PC preform after consolidation process. (c) CPE-PC fiber. (d) Roll of CPE film is placed into PC preform.

rolled around PTFE tube which as 15 mm diameter, and consolidated at 200 °C for 20 minutes. After that rolled CPE films were placed into consolidated PC preform as represented at Figure (d), resulted in CPE-PC core shell macroscopic rod in 15 mm and 30 mm diameters respectively. After that, thermal fiber draw process was conducted at 236 °C and volume reduction factor is specified to number of 75 which can be specified through division of macroscopic rod diameter to desired fiber diameter. As a result, meters of CPE-PC core-shell fibers which have 200 μ m and 400 μ m diameters respectively were successfully drawn. These fibers named as the step-1 fiber (Figure.2 (c)).

Furthermore, iterative size reduction technique was utilized to draw polymer encapsulated micro-nano fiber bundles. In this technique, rather than a second material roll, hundreds of drawn fibers (step 1) are placed into pre-consolidated preform (Figure (a)). Accordingly, number of 140 CPE-PC fibers were inserted into consolidated PSU preform which has 25 mm outside and 6 mm inside diameters. Afterwards, CPE-PC/PSU macroscopic rod was subjected thermal fiber draw process at 285°C resulted with CPE-PC/PSU core-shell fibers named as

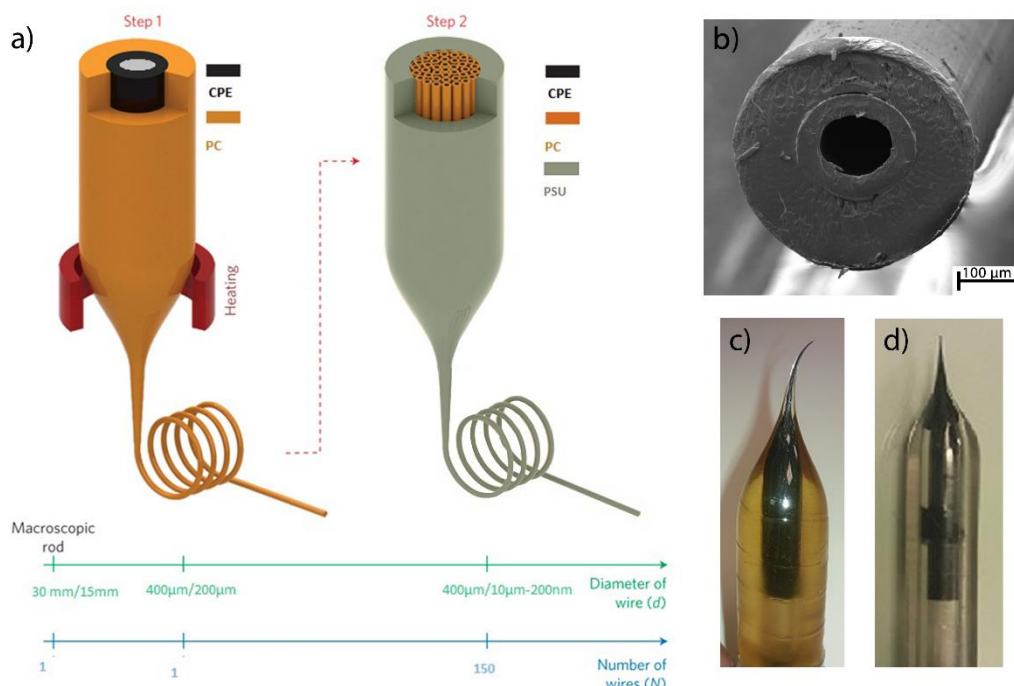


Figure 4.3: Iterative size reduction fiber drawing process. (a) Schematics of step-1 and step 2 fiber drawing. (b) SEM micrograph of step-1 CPE-PC core-shell fiber cross section. (c) Step-2 CPE-PC/PSU and (d) step-1 CPE-PC preforms after fiber drawing processes.

step-2 fibers. However, due to high glass transition temperature of PSU which is much above melting point of CPE, some CPE fibers were collapsed with each other. For this reason, second fiber drawing step were resulted with producing micro/nano dual scale fibers.

Besides conductive core-polymer encapsulated triboelectric fibers, metal-polymer core-shell fiber drawing was also investigated for TENG fabrics. It is worth to mention that most of metals have high melting points with respect to polymers makes unfeasible them for fiber drawing process. In parallel to this restrain, commercial solder alloys were preferred as a metal core material since they have relatively low melting point. Several analyses were performed through differential scanning calorimetry (DSC) in order to test melting points of different alloys resulted in chose of $\text{Pb}_{67}\text{Sn}_{33}$ alloy which has 224°C melting temperature. Accordingly, these commercial solder wires were melted within glass tube has 6 mm inside diameter in order to produce solder rod and also vaporize rosin substance which is presented in most of commercial solder alloys to help soldering process. Later on, PES preform in 20 mm outside and 6 mm inside diameters was consolidated at 240°C , 25 min and solder rod is inserted into preform. Fiber drawing process was optimized for number of 25 volume reduction factor resulted in production of $\text{Pb}_{67}\text{Sn}_{33}$ -PES core-shell fibers in approximately $224\ \mu\text{m}$ and $752\ \mu\text{m}$ outside diameters respectively.



Figure 4.4: Metal core-polymer encapsulated fibers. (a) Preparation of solder alloy rod. (b) End of fiber drawing process, melted solder rod within PSU preform. (c) SEM micrograph of $\text{Pb}_{67}\text{Sn}_{33}$ -PES core-shell fiber cross section.

4.2.2. Surface Modification and Device Fabrication

As represented in Figure 20, Ar plasma surface treatment leads to enhance output power characteristics of PC-PTFE based TENG. Accordingly, step 1 CPE-PC fibers were rolled over sample holder cylinders of plasma chamber to be exposed Ar plasma surface modification as represented at Figure (b). 2.4 GHz microwave source was used to plasma treatment along optimized power and reaction duration at 240 Watt and 5 min respectively. Ar gas was excessed at 50 sccm and cylinders were rotated at 6 rpm. After outer faces of fibers were exposed to plasma modification, same process was conducted to inner faces. Following to surface treatment of fiber, the proof of principle textile TENG was constructed through weaving of fibers with PTFE tape as represented in Figure (c).

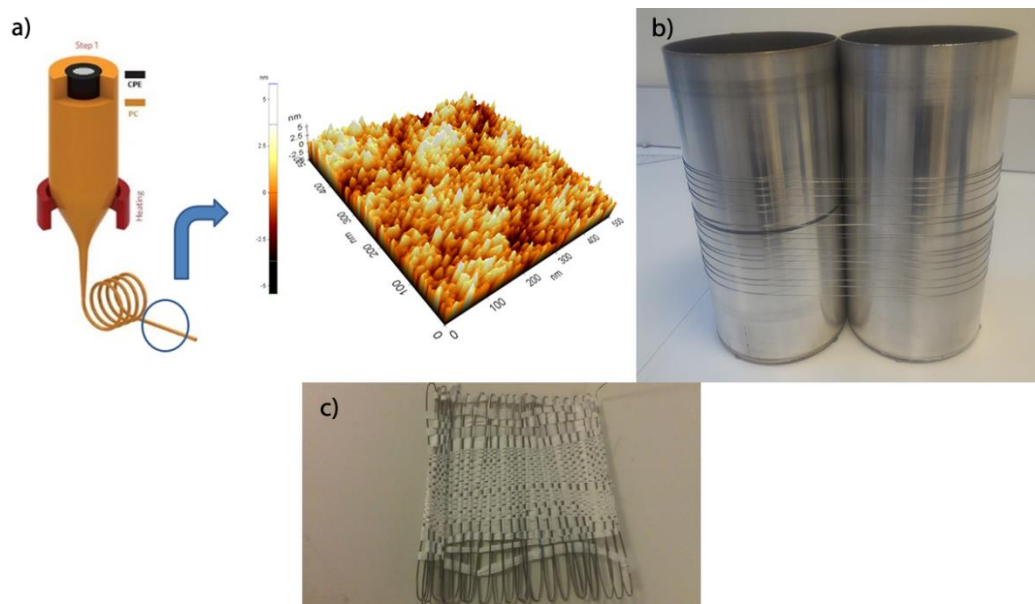


Figure 4.5: Surface modification for thermally drawn fibers and device structure. (a) Schematic of Ar plasma surface treatment on CPE-PC core-shell fiber. (b) Rolled fibers over plasma sample holder cylinders. (c) The proof of principle textile TENG.

4.3. Characterization

Output performance of woven structured textile TENG was characterized with respect to power generated device under external forces of custom made tapping machine. Short circuit current and open circuit voltage measurements were performed through Tektronix TDS-1012B Oscilloscope and Stanford SR-570 Current Preamplifier. Device was operated in single electrode mode where probes of measurement setups are attached woven structured single PC fiber in which CPE act as electrode structure and ground as a reference electrode. As represented at Figure, 21 μA and 340 peak to peak short circuit current and open circuit voltage respectively were measured. Moreover, textile TENG instantaneously powered up to 30 green LEDs through hand slapping. As a result, remarkable performance of the proof of principle textile TENG even it was operated at single electrode mode demonstrate that thermally drawn conductive core-polymer shell fibers would be promising structures for the construction of future textile based TENG.

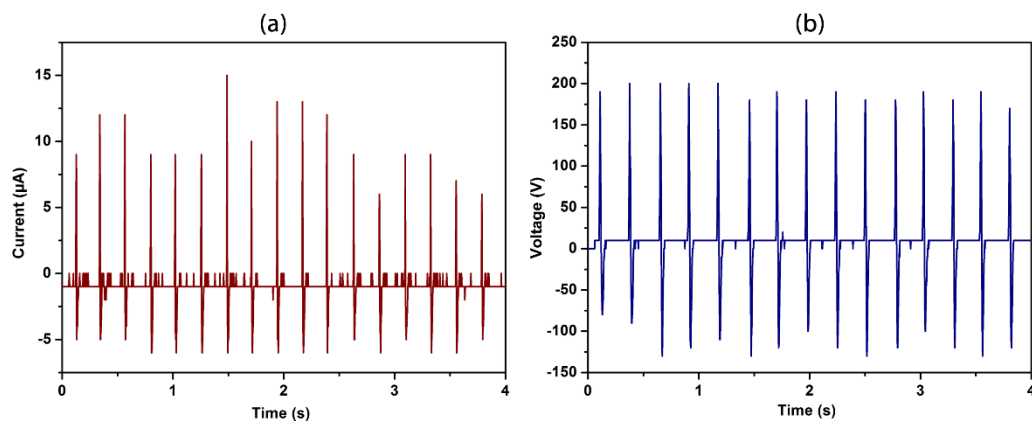


Figure 4.6: Output characteristics of textile TENG. Measurement results of (a) short circuits current, (b) open circuit voltage.

Chapter 5

Conclusions

5.1. Conclusion

In this study, considering promising energy harvesting and self-powered sensor capabilities of TENGs, we developed high performance biomechanical energy harvesting floor tiles based on CPE and PTFE triboelectric layers, which can instantaneously power 1400 commercial LEDs in single footstep. Device can generate 1.52 mA and 5.4 kV peak to peak short circuit current and open circuit voltage respectively at 7Hz tapping frequency. Biomechanical weight and motion sensor capability of TENG floor tiles was also investigated by weight based output characteristics of device which demonstrates that device can be used in security applications.

Behind the performance, fabrication process of TENG floor tiles offers novel perspectives to construct mass producible, low cost, large area and flexible TENG structures. In TENG research, CPE as a conductive polymer have been firstly used as a triboelectric layer which provides high performance for TENG output power owing to both efficient triboelectric charge generation and conductive properties of it. On the other hand, Ar plasma surface modification was also proposed as promising cost effective fabrication technique to build high performance massive TENG structures.

Besides the conventional TENG structures in which triboelectric layers are mostly in film formation, we have offered conductive core-polymer shell fibers based textile TENG structure. Accordingly, two different triboelectric fibers were fabricated through thermally fiber drawing technique as solder alloy-PES and metal-free CPE-PC core-shell fibers. The proof of principle textile TENG was constructed in single electrode mode through the combination of CPE-PC triboelectric fibers and PTFE tape and also Ar plasma surface treatment was exposed over fiber surfaces in order to enhance triboelectric properties of fibers. Device performance, where 21 μA and 340 peak to peak current and voltage were generated, and also instantaneously powered 16 LEDs, clearly demonstrated that triboelectric fibers are promising structures to build mass-producible, cost effective and flexible textile based TENGs.

5.2. Future Works

Utilizing Ar plasma surface treatment technique in fabrication TENG floor tiles have led to build large area and flexible TENG structures for large scale energy harvesting applications. Regarding about free and limitless mechanical energy source of winds and water sources such as rain drops, rivers and oceans, and promising scavenging capabilities of TENGs, cost-effective, mass producible large scale structures can be developed through Ar plasma surface modification technique.

Beside the effective fabrication feature of this technique, it is open to further theoretical investigations for triboelectric charge generation mechanism where we observed that Ar plasma surface modification changes triboelectric polarities of materials. A detailed XPS analysis are planned to investigate effect of Ar and other inert gases plasma treatment on triboelectric charge generation characteristics of materials.

Regarding to textile TENG, we consider promising features of mass-predictable, large scalable thermally drawn electrode core-polymer shell fibers. Accordingly, we are planning to build large area fabric TENG structures in free standing triboelectric layer mode where two different solder alloy electrode core-polymer shell fibers will be draw and weaved within each other. Sweaters, carpets and curtains can be built with these fabrics to harvest biomechanical energy into electricity and also fabric TENGs can be used as self-powered sensor in biomedical monitoring and electronic skin applications.

Bibliography

- [1] World Energy Council, “World Energy Resources 2016,” *World Energy Resources 2016*, 2016. .
- [2] A. G. Bailey, “The charging of insulator surfaces,” *Journal of Electrostatics*, vol. 51–52, no. 1–4, pp. 82–90, 2001.
- [3] D. J. Lacks and R. Mohan Sankaran, “Contact electrification of insulating materials,” *Journal of Physics D: Applied Physics*, vol. 44, no. 45, p. 453001, 2011.
- [4] F. Galembeck, T. A. L. Burgo, L. B. S. Balestrin, R. F. Gouveia, C. A. Silva, and A. Galembeck, “Friction, tribochemistry and triboelectricity: recent progress and perspectives,” *RSC Adv.*, vol. 4, no. 109, pp. 64280–64298, 2014.
- [5] L. S. McCarty and G. M. Whitesides, “Electrostatic charging due to separation of ions at interfaces: Contact electrification of ionic electrets,” *Angewandte Chemie - International Edition*, vol. 47, no. 12, pp. 2188–2207, 2008.
- [6] P. Iversen and D. J. Lacks, “A life of its own: The tenuous connection between Thales of Miletus and the study of electrostatic charging,” *Journal of Electrostatics*, vol. 70, no. 3, pp. 309–311, 2012.
- [7] P. M. Ireland, “Contact charge accumulation and separation discharge,” *Journal of Electrostatics*, vol. 67, no. 2–3, pp. 462–467, 2009.
- [8] B. Ravelo, F. Duval, S. Kane, and B. Nsom, “Demonstration of the triboelectricity effect by the flow of liquid water in the insulating pipe,” *Journal of Electrostatics*, vol. 69, no. 6, pp. 473–478, 2011.
- [9] S. Matsusaka, H. Fukuda, Y. Sakura, H. Masuda, and M. Ghadiri, “Analysis of pulsating electric signals generated in gas-solids pipe flow,” *Chemical Engineering Science*, vol. 63, no. 5, pp. 1353–1360, 2008.
- [10] J. Lowell and W. S. Truscott, “Triboelectrification of identical insulators.

- I. An experimental investigation,” *Journal of Physics D: Applied Physics*, vol. 19, no. 7, pp. 1273–1280, 1986.
- [11] K. M. Forward, D. J. Lacks, and R. M. Sankaran, “Triboelectric charging of granular insulator mixtures due solely to particle - Particle interactions,” *Industrial and Engineering Chemistry Research*, vol. 48, no. 5, pp. 2309–2314, 2009.
- [12] H. Watanabe *et al.*, “Triboelectrification of pharmaceutical powders by particle impact,” *International Journal of Pharmaceutics*, vol. 334, no. 1–2, pp. 149–155, 2007.
- [13] National Geographic, “Photos: Chile Volcano Erupts With Ash and Lightning,” 2008. [Online]. Available: <http://news.nationalgeographic.com/news/2008/05/photogalleries/volcano-photos/>. [Accessed: 20-Aug-2017].
- [14] NASA, “Phantoms From the Sand: Tracking Dust Devils Across Earth and Mars,” 2005. [Online]. Available: https://www.nasa.gov/vision/universe/solarsystem/2005_dust_devil.html. [Accessed: 20-Aug-2017].
- [15] C. P. R. Saunders, “A Review of Thunderstorm Electrification Processes,” *Journal of Applied Meteorology and Climatology*, vol. 32, pp. 642–655, 1993.
- [16] J. F. Kok and N. O. Renno, “Electrostatics in wind-blown sand,” *Physical Review Letters*, vol. 100, no. 1, 2008.
- [17] C. E. Krauss, M. Horányi, and S. Robertson, “Experimental evidence for electrostatic discharging of dust near the surface of Mars,” *New Journal of Physics*, vol. 5, 2003.
- [18] M. R. James, S. J. Lane, and J. S. Gilbert, “Volcanic plume electrification: experimental investigation of a fracture-charging mechanism,” *Journal of Geophysical Research*, vol. 105, no. B7, pp. 641–649, 2000.
- [19] A. P. Johnson, H. J. Cleaves, J. P. Dworkin, D. P. Glavin, A. Lazcano, and J. L. Bada, “The Miller Volcanic Spark Discharge Experiment,” *Science*, vol. 322, no. 5900, pp. 404–404, 2008.

- [20] J. C. Wilcke, “Disputatio physica experimentalis, de electricitatibus contrariis ...,” Typis Ioannis Iacobi Adleri ..., Rostochii, 1757.
- [21] P. E. Shaw, “Experiments on Tribo-Electricity. I. The Tribo-Electric Series,” *Proceedings of the Royal Society A*, vol. 94, pp. 16–33, 1917.
- [22] A. F. Diaz and R. M. Felix-Navarro, “A semi-quantitative tribo-electric series for polymeric materials: The influence of chemical structure and properties,” *Journal of Electrostatics*, vol. 62, no. 4, pp. 277–290, 2004.
- [23] G. S. P. Castle, “Contact charging between insulators,” *Journal of Electrostatics*, vol. 40–41, pp. 13–20, 1997.
- [24] W. D. Greason, “Investigation of a test methodology for triboelectrification,” *Journal of Electrostatics*, vol. 49, no. 3–4, pp. 245–256, 2000.
- [25] P. Llovera, P. Molinié, A. Soria, and A. Quijano, “Measurements of electrostatic potentials and electric fields in some industrial applications: Basic principles,” *Journal of Electrostatics*, vol. 67, no. 2–3, pp. 457–461, 2009.
- [26] Y. Zhang and T. Shao, “A method of charge measurement for contact electrification,” *Journal of Electrostatics*, vol. 71, no. 4, pp. 712–716, 2013.
- [27] A.-F. M. Seyam, Y. Cai, and W. Oxenham, “Devices for measuring electrostatic generation and dissipation on the surfaces of polymeric materials,” *Journal of The Textile Institute*, vol. 100, no. 4, pp. 338–349, 2009.
- [28] R. A. Lodge and B. Bhushan, “Effect of physical wear and triboelectric interaction on surface charge as measured by Kelvin probe microscopy,” *Journal of Colloid and Interface Science*, vol. 310, no. 1, pp. 321–330, 2007.
- [29] H. T. Baytekin, A. Z. Patashinski, M. Branicki, B. Baytekin, S. Soh, and B. A. Grzybowski, “The Mosaic of Surface Charge in Contact Electrification,” *Science*, vol. 333, no. 6040, pp. 308–312, 2011.
- [30] H. T. Baytekin, B. Baytekin, J. T. Incorvati, and B. A. Grzybowski,

- “Material transfer and polarity reversal in contact charging,” *Angewandte Chemie - International Edition*, vol. 51, no. 20, pp. 4843–4847, 2012.
- [31] T. A. L. Burgo, C. A. Silva, L. B. S. Balestrin, and F. Galembeck, “Friction coefficient dependence on electrostatic tribocharging,” *Scientific Reports*, vol. 3, no. 1, p. 2384, 2013.
- [32] M. W. Williams, “Triboelectric charging of insulating polymers-some new perspectives,” *AIP Advances*, vol. 2, no. 1, 2012.
- [33] D. J. Lacks, “The unpredictability of electrostatic charging,” *Angewandte Chemie - International Edition*, vol. 51, no. 28, pp. 6822–6823, 2012.
- [34] J. Lowell, “Contact electrification of metals,” *Journal of Physics D: Applied Physics*, vol. 8, no. 1, pp. 53–63, 1975.
- [35] J. Lowell and A. C. Rose-Innes, “Contact electrification,” *Advances in Physics*, vol. 29, no. 6, pp. 947–1023, 1980.
- [36] W. R. Harper, “The Volta Effect as a Cause of Static Electrification,” *Proceedings of the Royal Society A: Mathematical, Physical and Engineering Sciences*, vol. 205, no. 1080, pp. 83–103, 1951.
- [37] S. Matsusaka, H. Maruyama, T. Matsuyama, and M. Ghadiri, “Triboelectric charging of powders: A review,” *Chemical Engineering Science*, vol. 65, no. 22, pp. 5781–5807, 2010.
- [38] J. Lowell and W. S. Truscott, “Triboelectrification of identical insulators. II. Theory and further experiments,” *Journal of Physics D: Applied Physics*, vol. 19, no. 7, pp. 1281–1298, 1986.
- [39] T. J. Fabish and C. B. Duke, “Molecular charge states and contact charge exchange in polymers,” *Journal of Applied Physics*, vol. 48, no. 10, pp. 4256–4266, 1977.
- [40] A. F. Diaz and J. Guay, “Contact charging of organic materials: Ion vs. electron transfer,” *Journal of Research and Development, IBM*, vol. 37, no. 2, p. 249, 1993.
- [41] A. F. Diaz, “Contact electrification of materials: The chemistry of ions on polymer surfaces,” *American Chemical Society, Polymer Preprints, Division of Polymer Chemistry*, vol. 37, no. 2, pp. 64–65, 1996.

- [42] H. A. Mizes, E. M. Conwell, and D. P. Salamida, "Direct observation of ion transfer in contact charging between a metal and a polymer," *Applied Physics Letters*, vol. 56, no. 16, pp. 1597–1599, Apr. 1990.
- [43] L. S. McCarty, A. Winkleman, and G. M. Whitesides, "Ionic electrets: Electrostatic charging of surfaces by transferring mobile ions upon contact," *Journal of the American Chemical Society*, vol. 129, no. 13, pp. 4075–4088, 2007.
- [44] R. Zimmermann, S. Dukhin, and C. Werner, "Electrokinetic measurements reveal interracial charge at polymer films caused by simple electrolyte ions," *Journal of Physical Chemistry B*, vol. 105, no. 36, pp. 8544–8549, 2001.
- [45] P. B. Petersen and R. J. Saykally, "On the Nature of Ions At the Liquid Water Surface," *Annu. Rev. Phys. Chem.*, vol. 57, no. 23, pp. 333–64, 2006.
- [46] H. T. Baytekin, B. Baytekin, S. Soh, and B. A. Grzybowski, "Is Water Necessary for Contact Electrification?," *Angewandte Chemie International Edition*, vol. 50, no. 30, pp. 6766–6770, Jul. 2011.
- [47] W. R. Salaneck, A. Paton, and D. T. Clark, "Double mass transfer during polymer-polymer contacts," *Journal of Applied Physics*, vol. 47, no. 1, pp. 144–147, 1976.
- [48] J. Lowell, "The role of material transfer in contact electrification," *Journal of Physics D: Applied Physics*, vol. 10, no. 17, pp. L233–L235, 1977.
- [49] L. Lahti, "Electrostatic hazards in powder handling," *Journal of Hazardous Materials*, vol. 23, no. 2, p. 256, 1990.
- [50] S. Soh, S. W. Kwok, H. Liu, and G. M. Whitesides, "Contact De-electrification of electrostatically charged polymers," *Journal of the American Chemical Society*, vol. 134, no. 49, pp. 20151–20159, 2012.
- [51] H. T. Baytekin, B. Baytekin, T. M. Hermans, B. Kowalczyk, and B. A. Grzybowski, "Control of Surface Charges by Radicals as a Principle of Antistatic Polymers Protecting Electronic Circuitry," *Science*, vol. 341, no. 6152, pp. 1368–1371, 2013.
- [52] R. J. Van de Graaff, K. T. Compton, and L. C. Van Atta, "The Electrostatic

- Production of High Voltage for Nuclear Investigations,” *Physical Review*, vol. 43, no. 3, pp. 149–157, Feb. 1933.
- [53] L. B. Schein, “Recent advances in our understanding of toner charging,” *Journal of Electrostatics*, vol. 46, no. 1, pp. 29–36, 1999.
- [54] M. Lungu, “Electrical separation of plastic materials using the triboelectric effect,” *Minerals Engineering*, vol. 17, no. 1, pp. 69–75, 2004.
- [55] A. G. Bailey, “The science and technology of electrostatic powder spraying, transport and coating,” *Journal of Electrostatics*, vol. 45, no. 2, pp. 85–120, 1998.
- [56] Y. Kusano, S. Taormina, P. Michelsen, and K. Nakayama, “Triboplasma - its generation and application for surface modification,” 2008.
- [57] F. R. Fan, Z. Q. Tian, and Z. Lin Wang, “Flexible triboelectric generator,” *Nano Energy*, vol. 1, no. 2, pp. 328–334, 2012.
- [58] F. R. Fan, L. Lin, G. Zhu, W. Wu, R. Zhang, and Z. L. Wang, “Transparent triboelectric nanogenerators and self-powered pressure sensors based on micropatterned plastic films,” *Nano Letters*, vol. 12, no. 6, pp. 3109–3114, 2012.
- [59] S. Wang, L. Lin, and Z. L. Wang, “Nanoscale triboelectric-effect-enabled energy conversion for sustainably powering portable electronics,” *Nano Letters*, vol. 12, no. 12, pp. 6339–6346, 2012.
- [60] M. Kanik *et al.*, “A motion- and sound-activated, 3d-printed, chalcogenide-based triboelectric nanogenerator,” *Advanced Materials*, vol. 27, no. 14, pp. 2367–2376, 2015.
- [61] J. Chen *et al.*, “Harmonic-resonator-based triboelectric nanogenerator as a sustainable power source and a self-powered active vibration sensor,” *Advanced Materials*, vol. 25, no. 42, pp. 6094–6099, 2013.
- [62] Q. Liang *et al.*, “Recyclable and Green Triboelectric Nanogenerator,” *Advanced Materials*, vol. 29, no. 5, p. 1604961–n/a, Feb. 2017.
- [63] Z. H. Lin, G. Cheng, L. Lin, S. Lee, and Z. L. Wang, “Water-solid surface contact electrification and its use for harvesting liquid-wave energy,” *Angewandte Chemie - International Edition*, vol. 52, no. 48, pp. 12545–

12549, 2013.

- [64] W. Yang *et al.*, “Harvesting energy from the natural vibration of human walking,” *ACS Nano*, vol. 7, no. 12, pp. 11317–11324, 2013.
- [65] S. Wang, L. Lin, Y. Xie, Q. Jing, S. Niu, and Z. L. Wang, “Sliding-triboelectric nanogenerators based on in-plane charge-separation mechanism,” *Nano Letters*, vol. 13, no. 5, pp. 2226–2233, 2013.
- [66] G. Zhu *et al.*, “Linear-grating triboelectric generator based on sliding electrification,” *Nano Letters*, vol. 13, no. 5, pp. 2282–2289, 2013.
- [67] C. Zhang, T. Zhou, W. Tang, C. Han, L. Zhang, and Z. L. Wang, “Rotating-disk-based direct-current triboelectric nanogenerator,” *Advanced Energy Materials*, vol. 4, no. 9, 2014.
- [68] L. Lin *et al.*, “Segmentally structured disk triboelectric nanogenerator for harvesting rotational mechanical energy,” *Nano Letters*, vol. 13, no. 6, pp. 2916–2923, 2013.
- [69] P. Bai *et al.*, “Cylindrical rotating triboelectric nanogenerator,” *ACS Nano*, vol. 7, no. 7, pp. 6361–6366, 2013.
- [70] M. Zhang *et al.*, “Robust design of unearthed single-electrode TENG from three-dimensionally hybridized copper/polydimethylsiloxane film,” *Nano Energy*, vol. 30, pp. 155–161, 2016.
- [71] H. Zhang *et al.*, “Single-electrode-based rotating triboelectric nanogenerator for harvesting energy from tires,” *ACS Nano*, vol. 8, no. 1, pp. 680–689, 2014.
- [72] Z. H. Lin, G. Cheng, S. Lee, K. C. Pradel, and Z. L. Wang, “Harvesting water drop energy by a sequential contact-electrification and electrostatic-induction process,” *Advanced Materials*, vol. 26, no. 27, pp. 4690–4696, 2014.
- [73] R. Hinchet, W. Seung, and S. W. Kim, “Recent Progress on Flexible Triboelectric Nanogenerators for SelfPowered Electronics,” *ChemSusChem*, vol. 8, no. 14, pp. 2327–2344, 2015.
- [74] S. Niu *et al.*, “Theoretical investigation and structural optimization of single-electrode triboelectric nanogenerators,” *Advanced Functional*

Materials, vol. 24, no. 22, pp. 3332–3340, 2014.

- [75] S. Wang, Y. Xie, S. Niu, L. Lin, and Z. L. Wang, “Freestanding triboelectric-layer-based nanogenerators for harvesting energy from a moving object or human motion in contact and non-contact modes,” *Advanced Materials*, vol. 26, no. 18, pp. 2818–2824, 2014.
- [76] S. Niu *et al.*, “Theory of freestanding triboelectric-layer-based nanogenerators,” *Nano Energy*, vol. 12, pp. 760–774, 2015.
- [77] Y. Xie *et al.*, “Grating-structured freestanding triboelectric-layer nanogenerator for harvesting mechanical energy at 85% total conversion efficiency,” *Advanced Materials*, 2014.
- [78] S. Wang, S. Niu, J. Yang, L. Lin, and Z. L. Wang, “Quantitative measurements of vibration amplitude using a contact-mode freestanding triboelectric nanogenerator,” *ACS Nano*, vol. 8, no. 12, pp. 12004–12013, 2014.
- [79] G. Zhu *et al.*, “Harvesting water wave energy by asymmetric screening of electrostatic charges on a nanostructured hydrophobic thin-film surface,” *ACS Nano*, vol. 8, no. 6, pp. 6031–6037, 2014.
- [80] Z. Zhao *et al.*, “Freestanding Flag-Type Triboelectric Nanogenerator for Harvesting High-Altitude Wind Energy from Arbitrary Directions,” *ACS Nano*, vol. 10, no. 2, pp. 1780–1787, 2016.
- [81] S. Niu and Z. L. Wang, “Theoretical systems of triboelectric nanogenerators,” *Nano Energy*, vol. 14, pp. 161–192, 2014.
- [82] X. Wang, Z. L. Wang, and Y. Yang, “Hybridized nanogenerator for simultaneously scavenging mechanical and thermal energies by electromagnetic-triboelectric-thermoelectric effects,” *Nano Energy*, vol. 26, pp. 164–171, 2016.
- [83] Y. Hu, J. Yang, S. Niu, W. Wu, and Z. L. Wang, “Hybridizing triboelectrification and electromagnetic induction effects for high-efficient mechanical energy harvesting,” *ACS Nano*, vol. 8, no. 7, pp. 7442–7450, 2014.
- [84] H. Zhang *et al.*, “Triboelectric nanogenerator as self-powered active

- sensors for detecting liquid/gaseous water/ethanol,” *Nano Energy*, vol. 2, no. 5, pp. 693–701, 2013.
- [85] Q. Liang *et al.*, “Highly transparent triboelectric nanogenerator for harvesting water-related energy reinforced by antireflection coating,” *Scientific Reports*, vol. 5, no. 1, p. 9080, 2015.
- [86] C. Yao, A. Hernandez, Y. Yu, Z. Cai, and X. Wang, “Triboelectric nanogenerators and power-boards from cellulose nanofibrils and recycled materials,” *Nano Energy*, vol. 30, pp. 103–108, 2016.
- [87] J. Sun, W. Li, G. Liu, W. Li, and M. Chen, “Triboelectric Nanogenerator Based on Biocompatible Polymer Materials,” *The Journal of Physical Chemistry C*, vol. 119, no. 17, pp. 9061–9068, Apr. 2015.
- [88] K. Parida, V. Kumar, W. Jiangxin, V. Bhavanasi, R. Bendi, and P. S. Lee, “Highly Transparent, Stretchable, and Self-Healing Ionic-Skin Triboelectric Nanogenerators for Energy Harvesting and Touch Applications,” *Advanced Materials*, p. 1702181–n/a.
- [89] X. Cheng *et al.*, “Single-Step Fluorocarbon Plasma Treatment-Induced Wrinkle Structure for High-Performance Triboelectric Nanogenerator,” *Small*, vol. 12, no. 2, pp. 229–236, 2016.
- [90] H. Ryu *et al.*, “High-Performance Triboelectric Nanogenerators Based on Solid Polymer Electrolytes with Asymmetric Pairing of Ions,” *Advanced Energy Materials*, p. 1700289–n/a.
- [91] S. Wang *et al.*, “Maximum surface charge density for triboelectric nanogenerators achieved by ionized-air injection: Methodology and theoretical understanding,” *Advanced Materials*, vol. 26, no. 39, pp. 6720–6728, 2014.
- [92] W. Tang, C. Zhang, C. B. Han, and Z. L. Wang, “Enhancing Output Power of Cylindrical Triboelectric Nanogenerators by Segmentation Design and Multilayer Integration,” *Advanced Functional Materials*, vol. 24, no. 42, pp. 6684–6690, 2014.
- [93] Y. S. Zhou *et al.*, “Nanometer resolution self-powered static and dynamic motion sensor based on micro-grated triboelectrification,” *Advanced*

Materials, vol. 26, no. 11, pp. 1719–1724, 2014.

- [94] W. Song *et al.*, “Nanopillar Arrayed Triboelectric Nanogenerator as a Self-Powered Sensitive Sensor for a Sleep Monitoring System,” *ACS Nano*, vol. 10, no. 8, pp. 8097–8103, 2016.
- [95] Y. Zheng *et al.*, “An electrospun nanowire-based triboelectric nanogenerator and its application in a fully self-powered UV detector,” *Nanoscale*, vol. 6, no. 14, pp. 7842–6, 2014.
- [96] J. Chun *et al.*, “Mesoporous pores impregnated with Au nanoparticles as effective dielectrics for enhancing triboelectric nanogenerator performance in harsh environments,” *Energy Environ. Sci.*, vol. 8, no. 10, pp. 3006–3012, 2015.
- [97] S.-J. Park, M.-L. Seol, S.-B. Jeon, D. Kim, D. Lee, and Y.-K. Choi, “Surface Engineering of Triboelectric Nanogenerator with an Electrodeposited Gold Nanoflower Structure,” *Scientific reports*, vol. 5, no. May, p. 13866, 2015.
- [98] X. S. Zhang *et al.*, “Frequency-multiplication high-output triboelectric nanogenerator for sustainably powering biomedical microsystems,” *Nano Letters*, vol. 13, no. 3, pp. 1168–1172, 2013.
- [99] B. Meng *et al.*, “A transparent single-friction-surface triboelectric generator and self-powered touch sensor,” *Energy & Environmental Science*, vol. 6, no. 11, p. 3235, 2013.
- [100] C. K. Jeong *et al.*, “Topographically-designed triboelectric nanogenerator via block copolymer self-assembly,” *Nano Letters*, vol. 14, no. 12, pp. 7031–7038, 2014.
- [101] D. Kim, S. B. Jeon, J. Y. Kim, M. L. Seol, S. O. Kim, and Y. K. Choi, “High-performance nanopattern triboelectric generator by block copolymer lithography,” *Nano Energy*, vol. 12, pp. 331–338, 2015.
- [102] L. Zhang, L. Cheng, S. Bai, C. Su, X. Chen, and Y. Qin, “Controllable fabrication of ultrafine oblique organic nanowire arrays and their application in energy harvesting,” *Nanoscale*, 2014.
- [103] J. Yang, J. Chen, Y. Liu, W. Yang, Y. Su, and Z. L. Wang,

- “Triboelectrification-based organic film nanogenerator for acoustic energy harvesting and self-powered active acoustic sensing,” *ACS Nano*, vol. 8, no. 3, pp. 2649–2657, 2014.
- [104] C. Han, C. Zhang, W. Tang, X. Li, and Z. L. Wang, “High power triboelectric nanogenerator based on printed circuit board (PCB) technology,” *Nano Research*, vol. 8, no. 3, pp. 722–730, 2015.
- [105] L. Dhakar *et al.*, “Large Scale Triboelectric Nanogenerator and Self-Powered Pressure Sensor Array Using Low Cost Roll-to-Roll UV Embossing,” vol. 6, p. 22253, Feb. 2016.
- [106] X. Wang, S. Niu, Y. Yin, F. Yi, Z. You, and Z. L. Wang, “Triboelectric Nanogenerator Based on Fully Enclosed Rolling Spherical Structure for Harvesting Low-Frequency Water Wave Energy,” *Advanced Energy Materials*, vol. 5, no. 24, 2015.
- [107] T. Jiang *et al.*, “Structural Optimization of Triboelectric Nanogenerator for Harvesting Water Wave Energy,” *ACS Nano*, vol. 9, no. 12, pp. 12562–12572, 2015.
- [108] T. Jiang, Y. Yao, L. Xu, L. Zhang, T. Xiao, and Z. L. Wang, “Spring-assisted triboelectric nanogenerator for efficiently harvesting water wave energy,” *Nano Energy*, vol. 31, pp. 560–567, 2017.
- [109] A. Ahmed *et al.*, “Self-Powered Wireless Sensor Node Enabled by a Duck-Shaped Triboelectric Nanogenerator for Harvesting Water Wave Energy,” *Advanced Energy Materials*, vol. 7, no. 7, 2017.
- [110] J. Chen *et al.*, “Networks of triboelectric nanogenerators for harvesting water wave energy: A potential approach toward blue energy,” *ACS Nano*, vol. 9, no. 3, pp. 3324–3331, 2015.
- [111] Z. L. Wang, T. Jiang, and L. Xu, “Toward the blue energy dream by triboelectric nanogenerator networks,” *Nano Energy*, vol. 39, pp. 9–23, 2017.
- [112] Y. Yang *et al.*, “Triboelectric nanogenerator for harvesting wind energy and as self-powered wind vector sensor system,” *ACS Nano*, vol. 7, no. 10, pp. 9461–9468, 2013.

- [113] L. Zheng *et al.*, “A Hybridized Power Panel to Simultaneously Generate Electricity from Sunlight, Raindrops, and Wind around the Clock,” *Advanced Energy Materials*, vol. 5, no. 21, 2015.
- [114] Y. Fang *et al.*, “Solution processed flexible hybrid cell for concurrently scavenging solar and mechanical energies,” *Nano Energy*, vol. 16, pp. 301–309, 2015.
- [115] Y. Wu, X. Zhong, X. Wang, Y. Yang, and Z. L. Wang, “Hybrid energy cell for simultaneously harvesting wind, solar, and chemical energies,” *Nano Research*, vol. 7, no. 11, pp. 1631–1639, 2014.
- [116] S. Wang, X. Wang, Z. L. Wang, and Y. Yang, “Efficient Scavenging of Solar and Wind Energies in a Smart City,” *ACS Nano*, vol. 10, no. 6, pp. 5696–5700, 2016.
- [117] T. C. Hou, Y. Yang, H. Zhang, J. Chen, L. J. Chen, and Z. Lin Wang, “Triboelectric nanogenerator built inside shoe insole for harvesting walking energy,” *Nano Energy*, vol. 2, no. 5, pp. 856–862, 2013.
- [118] G. Zhu, P. Bai, J. Chen, and Z. Lin Wang, “Power-generating shoe insole based on triboelectric nanogenerators for self-powered consumer electronics,” *Nano Energy*, vol. 2, no. 5, pp. 688–692, 2013.
- [119] J. Zhong *et al.*, “Finger typing driven triboelectric nanogenerator and its use for instantaneously lighting up LEDs,” *Nano Energy*, vol. 2, no. 4, pp. 491–497, 2013.
- [120] X. Fan, J. Chen, J. Yang, P. Bai, Z. Li, and Z. L. Wang, “Ultrathin, rollable, paper-based triboelectric nanogenerator for acoustic energy harvesting and self-powered sound recording,” *ACS Nano*, vol. 9, no. 4, pp. 4236–4243, 2015.
- [121] R. Riemer *et al.*, “Biomechanical energy harvesting from human motion: theory, state of the art, design guidelines, and future directions,” *Journal of NeuroEngineering and Rehabilitation*, vol. 8, no. 1, p. 22, 2011.
- [122] R. I. H. and P.-A. F. and D. Briand, “Fully casted soft power generating triboelectric shoe insole,” *Journal of Physics: Conference Series*, vol. 773, no. 1, p. 12097, 2016.

- [123] J. Wang *et al.*, “Sustainably powering wearable electronics solely by biomechanical energy,” *Nature Communications*, vol. 7, p. 12744, 2016.
- [124] X. Pu *et al.*, “A self-charging power unit by integration of a textile triboelectric nanogenerator and a flexible lithium-ion battery for wearable electronics,” *Advanced Materials*, vol. 27, no. 15, pp. 2472–2478, 2015.
- [125] W. Seung *et al.*, “Nanopatterned textile-based wearable triboelectric nanogenerator,” *ACS Nano*, vol. 9, no. 4, pp. 3501–3509, 2015.
- [126] J. Chen *et al.*, “Micro-cable structured textile for simultaneously harvesting solar and mechanical energy,” *Nature Energy*, vol. 1, no. 10, p. 16138, 2016.
- [127] T. Zhou, C. Zhang, C. B. Han, F. R. Fan, W. Tang, and Z. L. Wang, “Woven structured triboelectric nanogenerator for wearable devices,” *ACS Applied Materials and Interfaces*, vol. 6, no. 16, pp. 14695–14701, 2014.
- [128] Y. Zi *et al.*, “Triboelectric-pyroelectric-piezoelectric hybrid cell for high-efficiency energy-harvesting and self-powered sensing,” *Advanced Materials*, vol. 27, no. 14, pp. 2340–2347, 2015.
- [129] S. Wang, Z. L. Wang, and Y. Yang, “A One-Structure-Based Hybridized Nanogenerator for Scavenging Mechanical and Thermal Energies by Triboelectric-Piezoelectric-Pyroelectric Effects,” *Advanced Materials*, vol. 28, no. 15, pp. 2881–2887, 2016.
- [130] S. Wang, L. Lin, and Z. L. Wang, “Triboelectric nanogenerators as self-powered active sensors,” *Nano Energy*, vol. 11, pp. 436–462, 2015.
- [131] W. Yang *et al.*, “Triboelectrification based motion sensor for human-machine interfacing,” *ACS Applied Materials and Interfaces*, vol. 6, no. 10, pp. 7479–7484, 2014.
- [132] J. Chen *et al.*, “Personalized keystroke dynamics for self-powered human-machine interfacing,” *ACS Nano*, vol. 9, no. 1, pp. 105–116, 2015.
- [133] Y. Yang *et al.*, “Human skin based triboelectric nanogenerators for harvesting biomechanical energy and as self-powered active tactile sensor system,” *ACS Nano*, vol. 7, no. 10, pp. 9213–9222, 2013.
- [134] Q. Zheng *et al.*, “In Vivo Self-Powered Wireless Cardiac Monitoring via

- Implantable Triboelectric Nanogenerator,” *ACS Nano*, vol. 10, no. 7, pp. 6510–6518, 2016.
- [135] Y. Ma *et al.*, “Self-Powered, One-Stop, and Multifunctional Implantable Triboelectric Active Sensor for Real-Time Biomedical Monitoring,” *Nano Letters*, vol. 16, no. 10, pp. 6042–6051, 2016.
- [136] P. Bai *et al.*, “Membrane-Based Self-Powered Triboelectric Sensors for Pressure Change Detection and Its Uses in Security Surveillance and Healthcare Monitoring,” *Advanced Functional Materials*, vol. 24, no. 37, pp. 5807–5813, 2014.
- [137] X. Pu *et al.*, “Ultrastretchable, transparent triboelectric nanogenerator as electronic skin for biomechanical energy harvesting and tactile sensing,” *Science Advances*, vol. 3, no. 5, p. e1700015, 2017.
- [138] X. Chen, T. Jiang, Y. Yao, L. Xu, Z. Zhao, and Z. L. Wang, “Stimulating Acrylic Elastomers by a Triboelectric Nanogenerator – Toward Self-Powered Electronic Skin and Artificial Muscle,” *Advanced Functional Materials*, vol. 26, no. 27, pp. 4906–4913, 2016.
- [139] H. Yu *et al.*, “A Self-Powered Dynamic Displacement Monitoring System Based on Triboelectric Accelerometer,” *Advanced Energy Materials*, 2017.
- [140] F. Yi *et al.*, “Self-powered trajectory, velocity, and acceleration tracking of a moving object/body using a triboelectric sensor,” *Advanced Functional Materials*, vol. 24, no. 47, pp. 7488–7494, 2014.
- [141] Y. K. Pang, X. H. Li, M. X. Chen, C. B. Han, C. Zhang, and Z. L. Wang, “Triboelectric Nanogenerators as a Self-Powered 3D Acceleration Sensor,” *ACS Applied Materials and Interfaces*, vol. 7, no. 34, pp. 19076–19082, 2015.
- [142] X. H. Li, C. B. Han, T. Jiang, C. Zhang, and Z. L. Wang, “A ball-bearing structured triboelectric nanogenerator for nondestructive damage and rotating speed measurement,” *Nanotechnology*, vol. 27, no. 8, p. 85401, 2016.
- [143] L. Lin *et al.*, “Triboelectric active sensor array for self-powered static and dynamic pressure detection and tactile imaging,” *ACS Nano*, vol. 7, no. 9,

pp. 8266–8274, 2013.

- [144] Y. Xi *et al.*, “Multifunctional TENG for Blue Energy Scavenging and Self-Powered Wind-Speed Sensor,” *Advanced Energy Materials*, vol. 7, no. 12, 2017.
- [145] Z. H. Lin *et al.*, “A self-powered triboelectric nanosensor for mercury ion detection,” *Angewandte Chemie - International Edition*, vol. 52, no. 19, pp. 5065–5069, 2013.
- [146] Z. H. Lin, G. Cheng, W. Wu, K. C. Pradel, and Z. L. Wang, “Dual-mode triboelectric nanogenerator for harvesting water energy and as a self-powered ethanol nanosensor,” *ACS Nano*, vol. 8, no. 6, pp. 6440–6448, 2014.
- [147] X. Li *et al.*, “Self-Powered Triboelectric Nanosensor for Microfluidics and Cavity-Confined Solution Chemistry,” *ACS Nano*, vol. 9, no. 11, pp. 11056–11063, 2015.
- [148] Y. Jie *et al.*, “Self-Powered Triboelectric Nanosensor with Poly(tetrafluoroethylene) Nanoparticle Arrays for Dopamine Detection,” *ACS Nano*, vol. 9, no. 8, pp. 8376–8383, 2015.
- [149] C. Zhang and Z. L. Wang, “Tribotronics—A new field by coupling triboelectricity and semiconductor,” *Nano Today*, vol. 11, no. 4, pp. 521–536, 2016.
- [150] C. Zhang, W. Tang, L. Zhang, C. Han, and Z. L. Wang, “Contact electrification field-effect transistor,” *ACS Nano*, vol. 8, no. 8, pp. 8702–8709, 2014.
- [151] C. Zhang, L. M. Zhang, W. Tang, C. B. Han, and Z. L. Wang, “Tribotronic logic circuits and basic operations,” *Advanced Materials*, vol. 27, no. 23, pp. 3533–3540, 2015.
- [152] C. Zhang, Z. H. Zhang, X. Yang, T. Zhou, C. B. Han, and Z. L. Wang, “Tribotronic Phototransistor for Enhanced Photodetection and Hybrid Energy Harvesting,” *Advanced Functional Materials*, vol. 26, no. 15, pp. 2554–2560, 2016.
- [153] C. Zhang *et al.*, “Organic Tribotronic Transistor for Contact-

- Electrification-Gated Light-Emitting Diode,” *Advanced Functional Materials*, vol. 25, no. 35, pp. 5625–5632, Sep. 2015.
- [154] Z. L. Wang, G. Zhu, Y. Yang, S. Wang, and C. Pan, “Progress in nanogenerators for portable electronics,” *Materials Today*, vol. 15, no. 12, pp. 532–543, 2012.
- [155] S. Niu *et al.*, “Theory of sliding-mode triboelectric nanogenerators,” *Advanced Materials*, vol. 25, no. 43, pp. 6184–6193, 2013.
- [156] S. Niu *et al.*, “Theoretical study of contact-mode triboelectric nanogenerators as an effective power source,” *Energy & Environmental Science*, vol. 6, no. 12, p. 3576, 2013.
- [157] B. Daglar *et al.*, “Anemone-like nanostructures for non-lithographic, reproducible, large-area, and ultra-sensitive SERS substrates,” *Nanoscale*, vol. 6, no. 21, pp. 12710–12717, 2014.
- [158] Z. Kolská, A. Řezníčková, V. Hnatowicz, and V. Švorčík, “PTFE surface modification by Ar plasma and its characterization,” in *Vacuum*, 2012, vol. 86, no. 6, pp. 643–647.
- [159] S. Zanini, R. Barni, R. Della Pergola, and C. Riccardi, “Modification of the PTFE wettability by oxygen plasma treatments: influence of the operating parameters and investigation of the ageing behaviour,” *Journal of Physics D: Applied Physics*, vol. 47, no. 32, p. 325202, 2014.
- [160] A. R. Akande and J. A. Adedoyin, “Correlation of charge transfer in metal/polymer contact with contact potential,” *Journal of Electrostatics*, vol. 51–52, no. 1–4, pp. 105–110, 2001.
- [161] J. C. Huang, “Carbon black filled conducting polymers and polymer blends,” *Advances in Polymer Technology*, vol. 21, no. 4, pp. 299–313, 2002.
- [162] L. Allison, S. Hoxie, and T. L. Andrew, “Towards seamlessly-integrated textile electronics: methods to coat fabrics and fibers with conducting polymers for electronic applications,” *Chemical Communications*, vol. 53, no. 53, pp. 7182–7193, 2017.
- [163] W. Zeng, L. Shu, Q. Li, S. Chen, F. Wang, and X. M. Tao, “Fiber-based

- wearable electronics: A review of materials, fabrication, devices, and applications,” *Advanced Materials*, vol. 26, no. 31. pp. 5310–5336, 2014.
- [164] K. Cherenack, C. Zysset, T. Kinkeldei, N. Münzenrieder, and G. Tröster, “Woven electronic fibers with sensing and display functions for smart textiles,” *Advanced Materials*, vol. 22, no. 45, pp. 5178–5182, 2010.
- [165] M. Stoppa and A. Chiolerio, “Wearable electronics and smart textiles: A critical review,” *Sensors (Switzerland)*, vol. 14, no. 7. pp. 11957–11992, 2014.
- [166] M. Yaman *et al.*, “Arrays of indefinitely long uniform nanowires and nanotubes,” *Nature Materials*, vol. 10, no. 7, pp. 494–501, 2011.
- [167] M. Bayindir, A. F. Abouraddy, J. Arnold, J. D. Joannopoulos, and Y. Fink, “Thermal-sensing fiber devices by multimaterial codrawing,” *Advanced Materials*, vol. 18, no. 7, pp. 845–849, 2006.
- [168] F. Sorin and Y. Fink, “Multimaterial multifunctional fiber devices,” *2009 35th European Conference on Optical Communication*, no. 1, pp. 3–6, 2009.
- [169] M. Bayandir *et al.*, “Metal – insulator – semiconductor optoelectronic fibres,” *Nature*, vol. 431, no. October, pp. 826–829, 2004.
- [170] F. Xi *et al.*, “Universal power management strategy for triboelectric nanogenerator,” *Nano Energy*, vol. 37, pp. 168–176, 2017.